GEOLOGY AND CONDITIONS OF FORMATION OF THE ZEOLITE-BEARING DEPOSITS SOUTHEAST OF ANKARA (CENTRAL TURKEY)

MUAZZEZ ÇELİK KARAKAYA[1],*, NECATİ KARAKAYA[1], AND FUAT YAVUZ[2]

[1] Selçuk Üniversitesi Mühendislik Fakültesi, Jeoloji Mühendisliği Böl. Konya, 42079, Türkiye
[2] İstanbul Teknik Üniversitesi, Maden Fakültesi, Jeoloji Müh. Böl. Maslak, 34469 İstanbul, Türkiye

Abstract—The pyroclastic sediments studied here contained varied amounts of zeolite and were formed in the saline alkaline Tuzgölü Basin following the alteration of dacitic volcanic materials during the Early to Late Miocene. The present study focused on the geological-geochemical properties of the zeolites and describes their formation. Mineralogical and chemical compositions were determined by X-ray diffraction, scanning electron microscopy, optical microscopy, and inductively coupled plasma mass spectrometry. Results indicated that the zeolitic tuffs consisted mainly of heulandite/clinoptilolite (Hul/Cpt), chabazite, erionite, and analcime associated with smectite. Smectite, calcite, and dolomite are abundant in the clay and carbonate layers which alternate with the zeolitic tuffs. K-feldspar, gypsum, and hexahydrite ($MgSO_4·6H_2O$) were also found in some altered tuffs and clay-marl layers as accessory minerals. The zeolite and other authigenic minerals showed weak stratigraphic zonation. Some vitric tuff layers contained no zeolite minerals and others were found to consist of almost pure Hul/Cpt and chabazite layers with economic potential. The rare earth elements (*REE*), large ion lithophile elements (LILE), and high-field strength elements (HFSE) in the Hul/Cpt-rich tuffs and vitric tuffs were enriched or depleted relative to the precursor rock, while many major elements were slightly or significantly depleted in all zeolitic tuffs. The amounts of *REE* in the chabazite- and erionite-rich tuffs were generally smaller than those in the precursor rock. The middle and heavy *REE* (*MREE* and *HREE*, respectively) were abundant in the Hul/Cpt-rich tuffs, tuffs, and smectitic bentonites. Chondrite-normalized *REE* values of the sample groups are characterized by sub-parallel patterns with enrichment in *LREE* relative to *HREE*. The mineral assemblages and geological setting indicated that zeolite diagenesis occurred in a saline-alkaline basin. The $\delta^{18}O$ and δD compositions of the Hul/Cpt, chabazite, and smectite indicated that the minerals formed at low to moderate temperatures and that some of the zeolitization occurred due to diagenetic alteration under closed-system conditions that varied according to the nature of the basin and with the composition and physical properties of the volcanic materials.

 Key Words—Analcime, Ankara, Chabazite, Clinoptilolite, Erionite, Heulandite, Smectite, Turkey, Zeolite.

INTRODUCTION

Zeolites are aluminosilicate minerals that form in a wide variety of geological environments or hydrological systems (closed or open) (Langella *et al*., 2001; Hay and Sheppard, 2001; Sheppard and Hay, 2001) by alteration of volcanic material under various geochemical conditions. Numerous studies have been conducted to investigate the origins of zeolites from volcanic materials of various compositions and nature and under different environmental conditions (Surdam, 1977; Hay, 1978; Iijima, 1978; Surdam and Sheppard, 1978; Gottardi, 1989; Hernandez *et al*., 1993; Sheppard and Hay, 2001; Snellings *et al*., 2008). Zeolite minerals are commonly formed from interactions of volcanic rocks and ash with water in open or closed saline-alkaline basins.

Well known zeolite deposits, especially of clinoptilolite, are found in western and northwestern Turkey.

The mineralogical, chemical, and physical properties of zeolite deposits from different regions of Turkey have been studied (Helvacı *et al*., 1993; Esenli and Özpeker, 1993; Temel and Gündoğdu, 1998; Gündoğdu *et al*., 1996; Esenli and Kumbasar, 1998; Kaçmaz and Koktürk, 2004; Esenli and Sirkecioğlu, 2005; Snellings *et al*., 2008). Turkey has approximately 50 million tons of zeolite reserves and, in the region of western Anatolia, these consist mainly of heulandite/clinoptilolite (Hul/Cpt). The zeolite deposits, formed in a saline alkaline lake environment, are associated with borates, clays, sodium and calcium-sulfate and carbonate minerals that have not been mined. Other zeolite deposits, exploited commercially, were formed from diagenetic alteration of rhyolitic and rhyodacitic tuff in Miocene pyroclastics (Esenli and Özpeker, 1993) and have abundant zeolite along with clay, feldspars, and quartz.

In the Tuzgölü Basin, the zeolite-bearing deposits are mainly interlayered with bentonite and in some places with carbonate-rich deposits. The Tuzgölü basin is shallow, closed, and fault-controlled, and surrounded by ophiolitic and carbonate rocks. Some of the tuff layers in the study area consist of almost pure Hul/Cpt

and chabazite, which represent between 40 and 95% (by weight) of the tuffs. The thickness, lateral continuity, and physical properties of these minerals also make exploitation of the deposits economically feasible. The geological features and occurrence of zeolite minerals with smectite and carbonate minerals indicate that different types of precursor volcanic rocks are found in this region. Some geological properties of chabazite-bearing deposits were determined in the study area by Şahin (2007); the origin of the zeolite minerals, the geochemical properties, and the environmental conditions were not determined, however. Karakaya *et al*. (2013) investigated the formation of two types of analcimes from the dehydration of volcanic and non-volcanic materials and determined their relationships with clinoptilolite.

Different zeolite minerals have different physical properties, including ion-exchange capacity, surface area, and pore-size distribution. These different properties result in varied applications, including use as filters, as chemical sieves, as additives to animal feed, in food and medicines, in odor removal, in molecular sieves (for the chemical industry), in water purification, in remediation, in fertilizers, in building materials, and in the removal of wastes or heavy metals from soil or water (Mumpton, 1999). Clinoptilolite and, to a lesser extent, chabazite are commonly occurring and readily available natural zeolite minerals which are used widely.

In the study area, some of the tuff layers have a greater percentage of Hul/Cpt and chabazite than found at other Turkish zeolite deposits. The occurrence of almost pure Hul/Cpt and its properties were examined primarily due to the scientific and industrial importance of Hul/Cpt and chabazite. The present study sought to: (1) investigate the mineralogical, geochemical, and morphological characteristics of the zeolite minerals in the study area; (2) explain the origin and environmental conditions of zeolites and clay minerals; and (3) determine the source rocks of the zeolites.

GEOLOGICAL SETTING

The study area is located ~80 km south of Ankara in central Anatolia and in the Tuzgölü Basin, a Tertiary lacustrine basin that contains widespread volcanic and volcaniclastic rocks ranging from dacite to basalt interlayered with sedimentary rocks (Temel *et al*., 1998). The Tuzgölü Basin is a fore-arc basin which developed during the Late Cretaceous−Tertiary (Görür *et al*., 1984; Okay *et al*., 2001; Gürer and Aldanmaz, 2002) (Figure 1). The oldest geological units were described by Karakaya *et al*. (2012). The early Miocene sediments of the Aktepe Formation consist of conglomerate (at the base) interbedded with sandstone, siltstone, claystone, marl, and limestone. The formation grades laterally and vertically into the Karacadağ volcanites in the upper levels of the sequence (Figure 2). The basin

was a closed lacustrine basin during the Miocene–Quaternary. Major tectonic movements affected the Anatolian plate during the Late Miocene−Pliocene (Uğuz *et al.*, 1999), and volcanic rocks which were predominantly calc-alkaline are found above the oceanic slab of the Afro-Arabian plate (Innocenti *et al.*, 1975; Pasquar *et al.*, 1988). The Late Miocene volcanites west and southwest of the basin are of mainly high-K calc-alkaline compositions. The volcanic rocks consist largely of pyroclastic deposits and lava domes with basaltic, andesitic, and dacitic compositions following several episodes of Karacadağ volcanism. Miocene–Pliocene fluvial-lacustrine carbonates and clay beds are partially intercalated with the pyroclastics (mainly zeolitic tuff) but less commonly with the lava layers. The zeolite-rich tuffs are located mainly in the upper strata of the Aktepe Formation, with some found in the Karacadağ pyroclastics, and they are associated with detrital and chemical (carbonate) sedimentary rocks (Figure 2). Zeolite mineralization was not observed in tuffs that were not intercalated with sedimentary rocks. The volcanism occurred in the Middle Miocene (19 to 18 Ma) (Kurt *et al*., 2008), and the Aktepe Formation was deposited before the Karacadağ volcanism. All the older units are unconformably overlain by Pliocene–Quaternary alluvium (Figure 2).

MATERIALS AND METHODS

Samples were collected from different sections and random locations in the study area (Figure 2). All of the samples were ground gently for 5 min in a porcelain ball mill prior to X-ray diffraction (XRD) and chemical analysis.

Mineralogical analysis was performed at Hacettepe University (Ankara, Turkey) with XRD using randomly oriented samples (Rigaku D/MAX 2200 PC, Japan, CuKα radiation, 40 kV and 40 mA, and a scanning speed of 2º/min from 2 to 70º2θ). The <2 μm clay fraction was obtained by the gravitational sedimentation of the samples and then separated by centrifugation. The fractionated 50−60 g samples in 250 mL polyethylene centrifuge bottles were centrifuged at $1620 \times g$ using a Jouan C4i (France) centrifuge. Following removal of the non-silicate minerals (*e.g.* calcite and dolomite) from the clay-sized fractions, three specimens of each sample were prepared for XRD analysis by sedimentation onto glass slides with air-drying at 25ºC. To remove carbonate minerals from the samples, dilute (5%) HCl acid solution was added slowly to the sample beaker until the reaction stopped at 30ºC (Tucker, 1988, and references therein). Then the sample was washed several times with distilled water and transferred to a measuring cylinder; 500 mL of deionized water was added to the sample. The three slides prepared were subjected to: (1) no further treatment; (2) ethylene glycol solvation; and (3) heating at 490ºC for 4 h, respectively. Mineral proportions were determined from the powder XRD
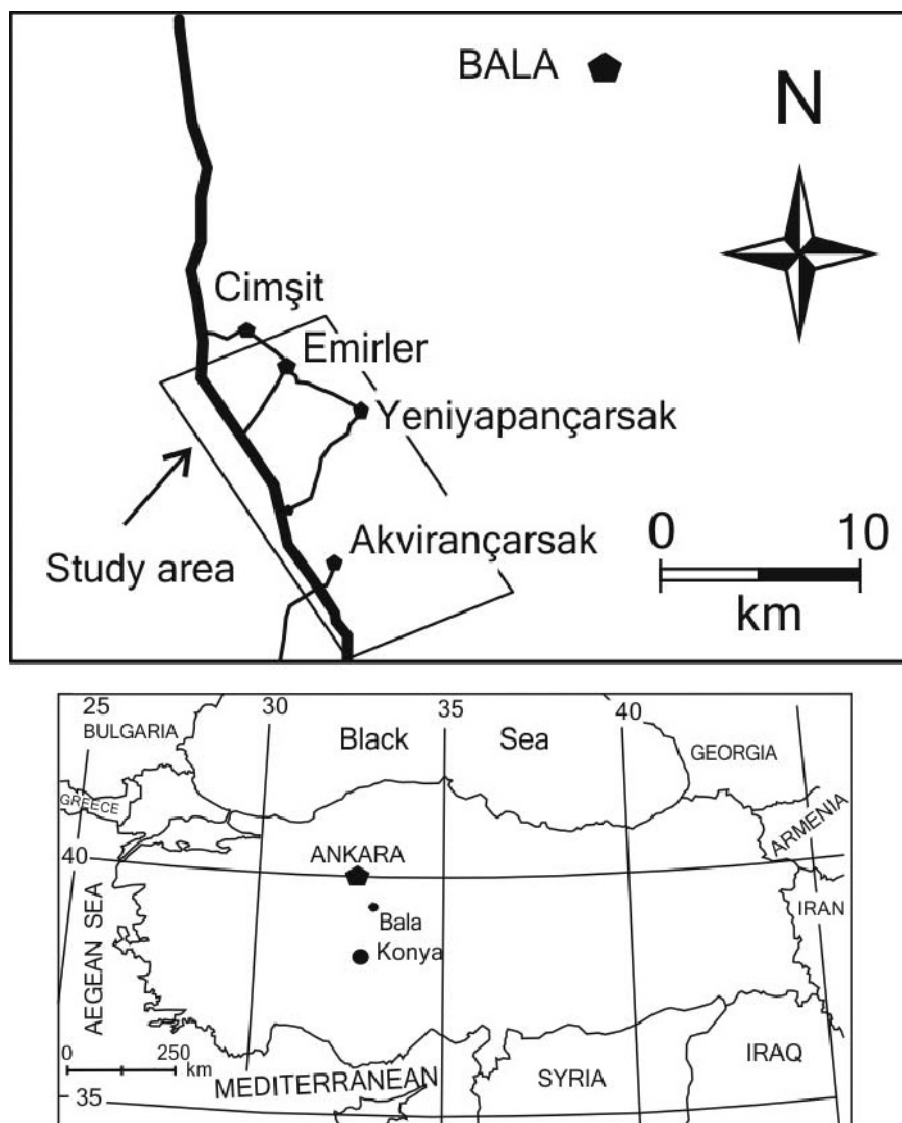
Figure 1. Location map showing Ankara, Konya, and other locations in the study area. The study area is located in the southeastern part of the Tuzgölü Basin in central Anatolia.

patterns according to the external standard method developed by Gündoğdu (1982) and from a combined chemical analysis (Table 1). All samples were mounted as described by Temel and Gündoğdu (1996) and Gündoğdu (1982), and the characteristic peak intensities (I) of the minerals were normalized to those of the (104) reflection of dolomite. The K factor was determined for each mineral (including clays with peaks between 19 and 20º2θ) by weight in a 1:1 dolomite-mineral mixture as follows: $K = I_{dolomite}/I_{mineral}$. The mineral percentages were calculated from the following equation: % of mineral $a = (100 \times K_a \times I_a)/(K_a \times I_a + K_b \times I_b + ... K_n \times I_n)$. The method was accurate to within ±15%.

The sizes and morphological features of the submicroscopic zeolite minerals and their interrelations with other minerals were determined using scanning electron microscopy (SEM). Elemental compositions were determined by energy-dispersive X-ray spectroscopy (EDS). The LEO 1430VP (Zeiss Cambridge, UK) SEM at Afyonkarahisar Kocatepe University was used to identify the mineral composition using an accelerating voltage of 15−20 kV with a beam current of 15 mA and a spot size of 5 μm. The sample was placed in a sample holder, dried at 50ºC for 1 h and coated with 5 μm of gold before EDS analysis. A ZAF calculation program was used to calculate the wt.% of the major oxides at each point.

The total abundances of the major oxides and the minor, rare-earth, and refractory elements of the rock samples were determined by ACME Laboratories
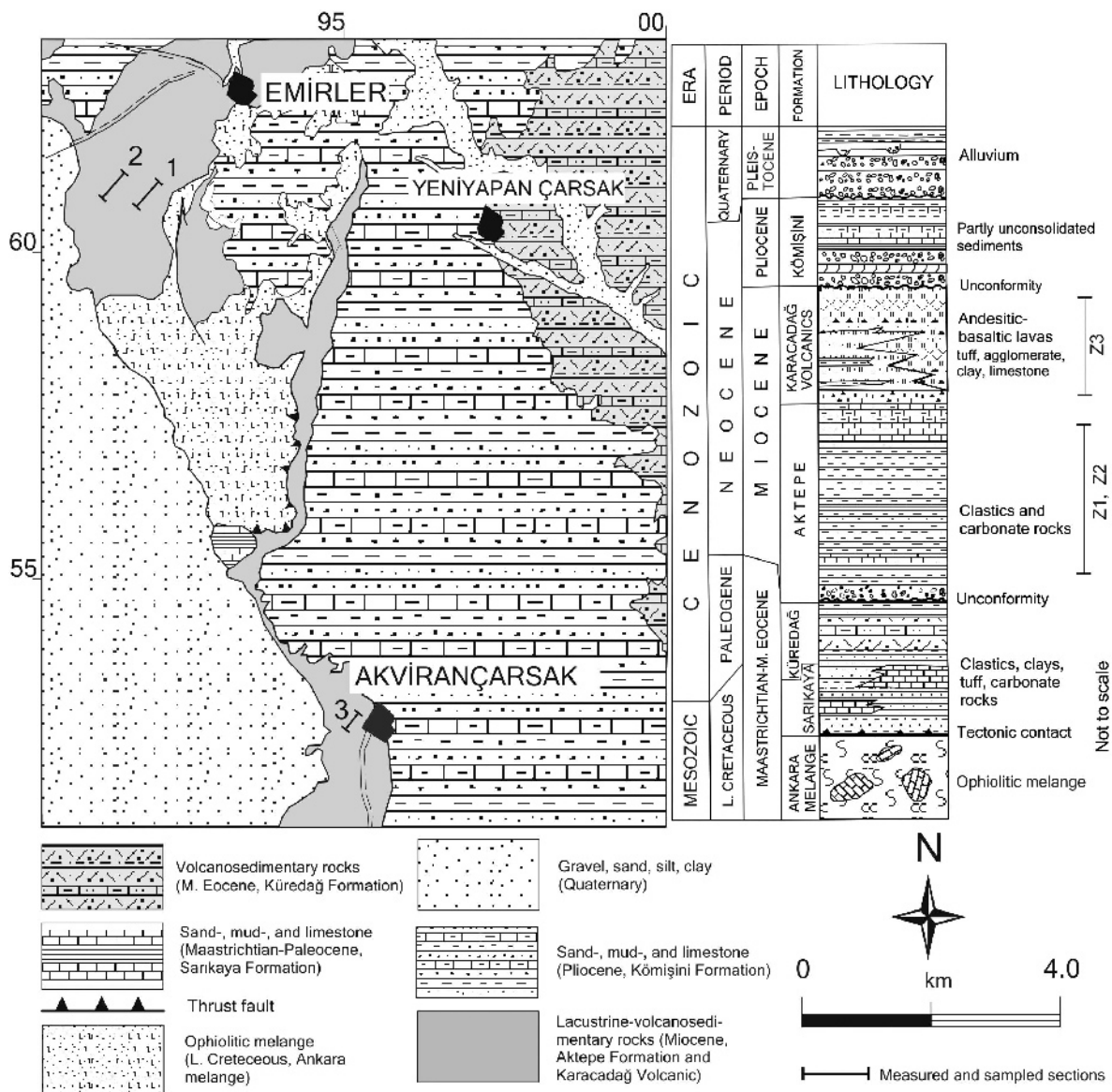
Figure 2. Map showing the geology, generalized stratigraphic sections (simplified from the MTA 1:100,000 scale map and Uğuz *et al*., 1999) and sample localities in the study area.

Table 1. Mineral composition of the sections presented in terms of maximum values (wt.%) (sparsely abundant components were omitted).

Sections	Sme	Anl	Dol	Cal	Ksp	Mi/Ilt	Kln	Qz/Opl	Hul/Cpt	Eri	Cbz	Gp	Hl	Hex
Z0	⩽52		⩽18	⩽74	⩽33	⩽18		⩽19	⩽70	⩽65				
Z3	⩽63	⩽20	⩽82	⩽52	⩽50	⩽11	⩽21	⩽60	⩽92	⩽40				
Z4	⩽85	⩽8	⩽2	⩽10	⩽73	⩽8	⩽6	⩽18	⩽36	⩽16	⩽94	⩽6	⩽3	
Z5	⩽70	⩽20	⩽77	⩽50	⩽21	⩽10	⩽9	⩽16	⩽33	⩽42	⩽67	⩽8	⩽5	⩽45

Ab: albite, Anl: analcime, Mi: mica, Cal: calcite, Cbz: chabazite, Dol: dolomite, Eri: erionite, Fsp: feldspar, Gp: gypsum; Hex: hexahydrite; Hul/Cpt: heulandite/clinoptilolite, Hl: halite; Ilt: illite; Kln: kaolinite, Qz/Opl: Quartz, opal-CT, Ksp: feldspar (most abbreviations from Whitney and Evans, 2010).

(Vancouver, British Columbia, Canada) using inductively coupled plasma optical emission spectrometry (ICP-OES) and mass spectrometry (ICP-MS) (Spectro ICP-OES and Perkin Elmer ELAN 9000 ICP-MS, USA, respectively). Samples (0.1 g) were fused in Li-metaborate/tetraborate and digested with nitric acid. Loss on ignition (LOI) was determined as the weight difference after ignition at 1000ºC. The total organic carbon (TOC) and sulfur concentrations were also measured by ACME Laboratories (LECO CS230). In addition, a separate 0.5 g portion of each sample was digested in aqua regia and analyzed by ICP-MS to determine the precious- and base-metal contents (*e.g.* Al, Fe, Ti, Co, Cd, Zr, Ga, and Nb).

Stable isotope analyses ($\delta^{18}O$ and δD) of the Hul/Cpt, analcime, chabazite, and smectite were conducted on zeolite-rich, smectite and calcite- and dolomite-containing samples. The smectite was obtained from the <2 μm clay fraction using the methods described above, and the zeolite-rich samples were separated from feldspar and quartz using the heavy-liquid method described by Ming and Dixon (1987). A mixture of tetrabromoethane and bromobenzene was used as the heavy liquid, and the specific gravity of the liquid was adjusted to 2.28 g/cm^3.

Stable isotope analyses of the samples were performed at the National Isotope Center (New Zealand). The mineral samples were analyzed using a HEKAtech high temperature elemental analyzer equipped with a Merhantek Model 300 CO_2 laser and coupled with a GV Instruments IsoPrime isotope ratio mass spectrometer (IRMS) (Isoprime, UK). In the ^{18}O measurement method, the samples are ground to <2 μm clay-size powder and weighed into a sample holder made of stainless steel with 36 holes drilled into it. The sample and standards were placed in the chamber and baked at 200ºC for 3−4 days before transfer to the vacuum chamber while still hot. Once under high vacuum, an aliquot of BrF$_5$ was allowed into the chamber (to remove any moisture and organics and to prepare the surface for analysis), at room temperature, for 24 h. The BrF$_5$ was then pumped away and the sample left under vacuum for a further 24 h. Under heating, dehydration of the zeolite would have commenced. The laser, positioned over the sample chamber which can be moved in XY directions in order to align the sample to be analyzed, was then fired at the sample in a BrF$_5$-rich atmosphere. The residual gas in the chamber was opened up to an evacuated Kel-F trap which was cooled in liquid nitrogen; the gas was allowed to stay in this trap for 1.5 min and then was opened up to a second Kel-F trap for 1.5 min. This was then opened to allow what was left to pass over the top of a mercury diffusion pump which behaves as a 'getter'. The cleaned up oxygen was converted to CO_2 on a hot platinized graphite target and the CO_2 was trapped cryogenically; non-condensable volatiles were pumped away. The CO_2 was allowed back into gas form so that the yield could be measured and then frozen into the sample bottle ready to

go to the IRMS for analysis to leave O_2 which was converted to CO_2 on hot graphite. The oxygen yields were recorded, and the CO_2 gas analyzed using a Geo20-20 mass spectrometer (The Sercon Group, UK). The precision of the standards was 1.5‰, and oxygen was extracted from the sample powders for isotope analysis using a CO_2 laser and BrF$_5$ as described above (Sharp, 1990). The oxygen isotope values were reported in the common $\delta^{18}O$ notation relative to Vienna Standard Mean Ocean Water (VSMOW). The samples were normalized to the international quartz standard NBS 28 using a value of +9.6‰. The target is normally loaded with at least three NBS28 standards (four in the present case) as well as several secondary standards. This extraction process is manual and is very time consuming, often taking 2−3 days to complete, and standards are extracted at the beginning and end of each day. At least one sample was run in duplicate each day and the four NBS 28 standards analyzed with the samples here varied by <0.15‰.

For the deuterium measurement, the powdered samples were weighed into a silver capsule and stored in an oven at 200ºC for 3−4 days, then transferred to a zero blank auto-sampler which was flushed with helium for 2−3 min. The sample rested in the auto-sampler helium atmosphere for 12 h before being dropped into a 1450ºC furnace. All of the samples were analyzed in triplicate. The results were reported with respect to VSMOW, normalized to the international standards IAEA-CH-7, NBS 30, and NBS 22, and reported with δD values of −100‰, 66‰ and 118‰, respectively.

RESULTS

Field observations

Detailed examination of the lithological properties and thicknesses of the tuff, mudstone, and carbonaceous sand- and siltstone layers revealed that the stratification and interlayering were inhomogeneous (Figure 3). Stratigraphically, sections Z4 and Z5 passed vertically to section Z3, and sections Z4 and Z5 showed a lateral transition into each other. The mudstone and marl beds were pale green to beige, a few centimeters to a few meters thick, and were often compacted, especially when they alternated with tuff and slightly carbonate-rich beds. The thickness of the carbonate layers increased to as much as 3−5 m thick toward the upper part of the sequence. Thin alluvial sediments (5−10 cm) consisting of silt, sandstone, and minor conglomerate covered some of the tuffs and other lithologies and were eroded in the upper portions of the sequence. The volcaniclastic sediments were commonly absent in the upper levels of the Aktepe Formation, and the spatial distribution of the volcanoclastics was dependent on the structural conditions (section Z3) (Figure 3).

The volcanic activity in the area generated ash, pumice, and welded ignimbrite. The zeolitized tuffs
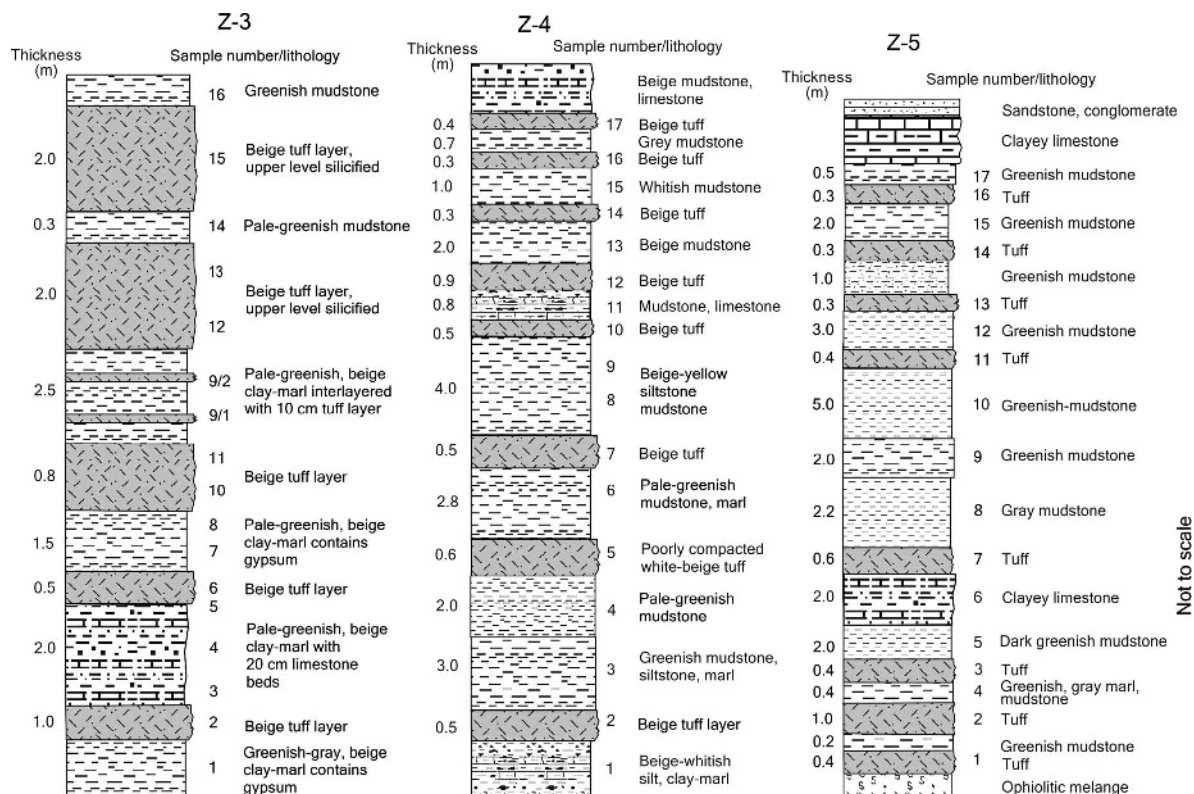
Figure 3. Generalized stratigraphic column of the Aktepe Formation and Karacadağ volcano-sedimentary rocks. The figure also shows the detailed stratigraphic section of the interval sampled in this study. The measured sections compiled at localities 3, 4, and 5 show the lithologies of the sampled units.

were mainly interlayered with clay, marl, limestone, and siltstone and/or sandstones that were deposited together in a lacustrine environment (Figures 2, 3). The volcanic components were abundant, especially in the clay and siltstone, but were only sparsely distributed in the limestone. The marl and limestone layers were truncated laterally by erosion surfaces. The Hul/Cpt-rich tuff layers were between 0.2 and 2.0 m thick, and the clay layers were between 0.2 and 2.2 m thick. Hul/Cpt-bearing tuffs and tuffites were identified in the upper levels of the Aktepe Formation and Karacadağ volcanites with inter-calated clay beds (Figures 2, 3). The alternating tuffitic, psammitic, pelitic, silty, and carbonate layers were characterized by irregular layer thickness and intercala-tion (Figure 3). Zeolite minerals other than analcime were mainly found in the tuff/tuffite layers in some regions and were interlayered with dark green smectite-rich clays. Visible gypsum crystals (1−4 cm across) occur in some clay layers, and the base of the Aktepe Formation consists mainly of pale green to beige, slightly silty, hard and tightly-cemented carbonate layers and clay-rich beds with conchoidal and subconchoidal fractures. The sedimentary rocks in the upper levels of the Aktepe Formation alternate with closely or loosely compacted, thin to moderately thick (1−10 cm) carbonate layers and white to beige tuff layers. The Hul/Cpt-rich tuff layers

alternated with the mudstone (Figure 3). Silica-rich beds or lenses were found between the Hul/Cpt-rich tuff layers, and zeolite minerals were commonly found in smectitic bentonite layers that alternate with lacustrine sediments. The volcano-sedimentary beds dipped at between 25 and 65º NW due to tectonic deformation and were folded and fractured. In locations with significant tectonic deforma-tion, the tuff-tuffite layers had a limited lateral continuity of 50 to 200 m.

Mineralogy-petrography

Zeolite minerals usually occur as microcrystalline aggregates (1.0−30 µm) that are generally associated with smectite, feldspar, silica, and some carbonate minerals and less commonly with gypsum (Table 1, Figure 4). Halite and hexahydrite minerals were sparsely distributed and mostly within ~50 m of lateral continua-tion of the section Z5. The lower part of this sequence is rich in dolomite, K-feldspar, and smectite, whereas zeolite-rich lithologies were more common in the upper part of the sequence. Hul/Cpt was mainly observed with erionite, sometimes with chabazite and rarely with analcime in the upper part of the sequence. Smectite, calcite, and/or dolomite were the most common and abundant non-zeolite minerals in the clay, silt, and carbonate layers. Albite, quartz, mica (mostly, in
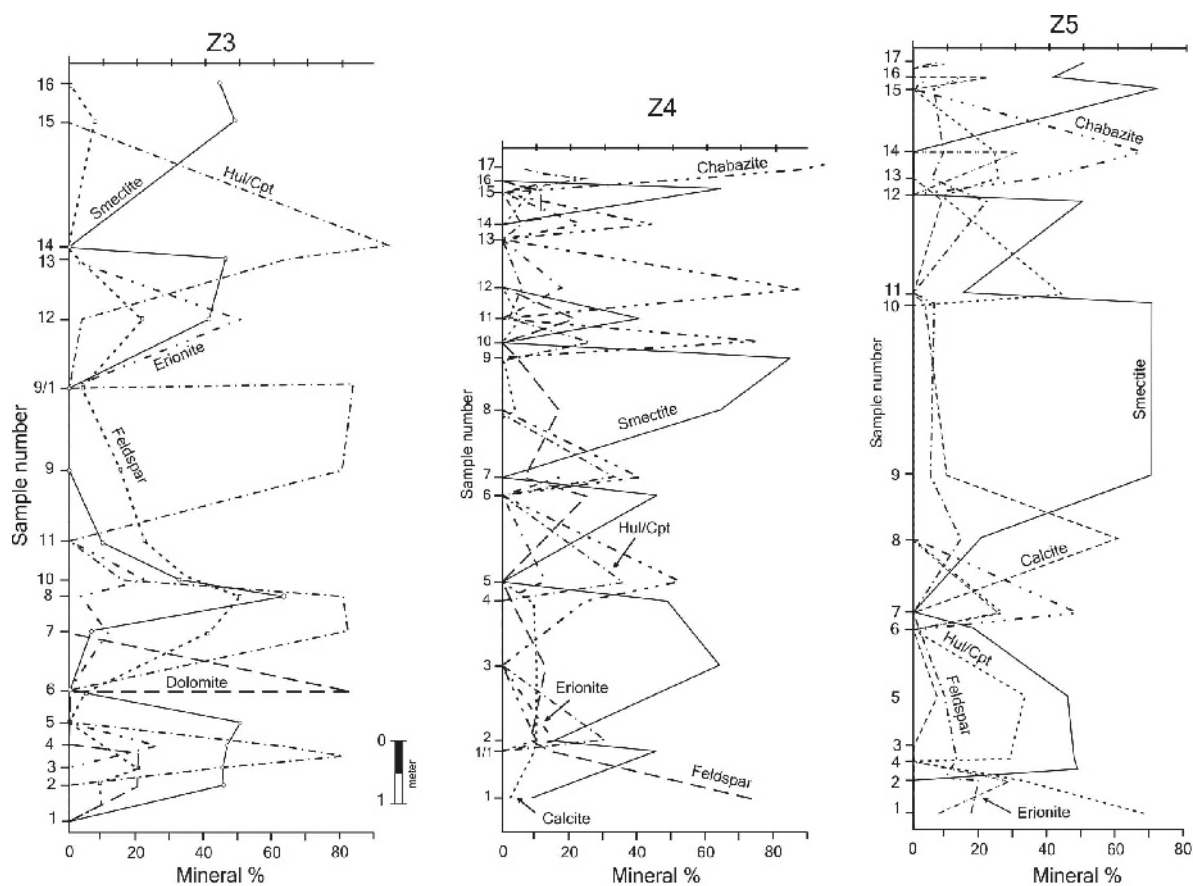
Figure 4. Measured sections compiled at localities Z3, Z4, and Z5, showing the mineral contents of the sampled units.

mudstones, illite), and kaolinite were also present in the layers (Table 1, Figure 4), and clay, silt, and carbonate layers were interlayered with the zeolitic tuffs. The upper part of the sequence generally resulted from calcite-rich carbonate rocks and sandstones composed of detrital minerals.

Vitrophyric and partially porphyric textures were identified in the ignimbrite and lava samples. The most significant phenocrysts were distinctly zoned and twinned andesine−oligoclase (An$_{15-40}$ determined from the extinction angles using the Michel-Levy method) showing neoformed K-feldspar and plagioclase, resorbed and fractured quartz, some biotite (Figure 5a), and small amounts of amphibole in the ignimbrite samples. Significant amounts of K-feldspar were present, especially at the bottom level of the section Z3, and smaller amounts at intermediate levels of Z4. The plagioclase and K-feldspar are fresh but the biotite and amphibole showed evidence of chloritization and oxidation. Consistent with the types, amounts, and textural characteristics of the phenocrysts, the ignimbrites are dacitic, andesitic, and trachytic in composition.

The glassy matrix was mostly welded and sometimes showed signs of devitrification; the crystal size was too small to be defined by microscopic examination, however.

Pumice fragments, spherulites, and elongated, sharp, and platy shards of glass were observed, and pieces of glass, splinters, and acicular and prismatic crystals formed from pumice and fibrous chalcedony are present.

The most common zeolite mineral is Hul/Cpt, which was present at different proportions in the groundmass and/or replacing glass and sometimes feldspars. Platy Hul/Cpt crystals, fibrous erionite, sparsely abundant twinned and zoned feldspar crystals, quartz, and volcanic glass were observed in the Hul/Cpt-rich samples (Figures 5b-d). The microcrystalline (<0.1 μm) Hul/Cpt crystals are equal in size, occasionally radial, clear in transmitted light, and show low relief and near parallel extinction (Figures 5b,c). Chabazite and analcime were not identified in thin section.

The zeolite-rich tuff samples consist of five zeolite mineral associations with or without non-zeolite minerals in different quantities from the bottom to the top of the sequence: (1) Hul/Cpt + analcime ± erionite; (2) Hul/Cpt + erionite (or offretite); (3) Hul/Cpt + erionite (or offretite) + chabazite; (4) Hul/Cpt, and (5) chabazite (Table 1, Figures 4, 5, 6). Hul/Cpt and chabazite were the most abundant zeolite minerals in some of the tuff layers (Figure 6). Opal-CT was identified by two peaks at 20−22º2θ.
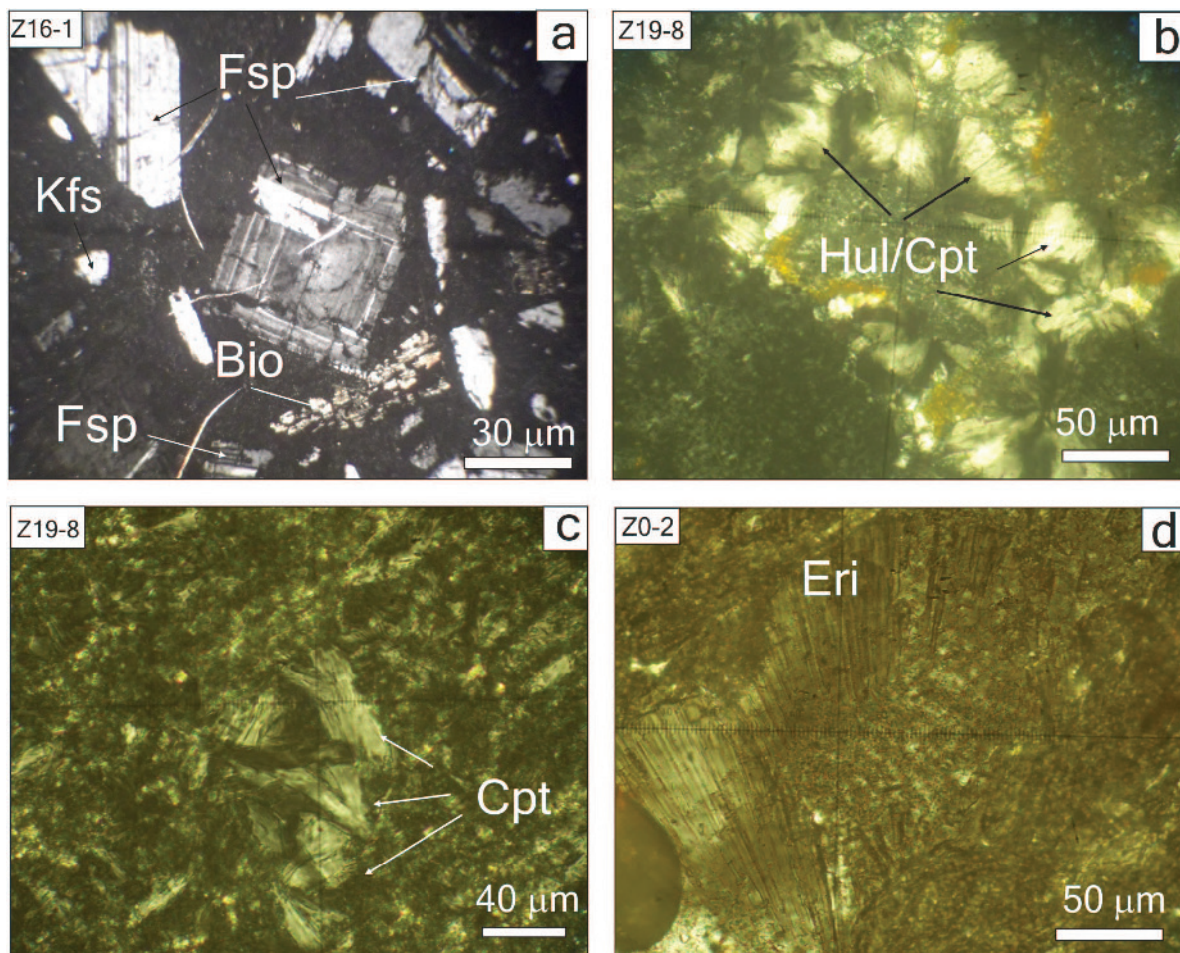
Figure 5. Photomicrographs of the vitrophyric and partially porphyric textures of the lava samples in reflected polarized light (a). Distinctly twinned plagioclase of mostly andesine−oligoclase composition, K-feldspar, and minor biotite in groundmass. Platy Hul/ Cpt crystals of the same size, fibrous and partially radial erionite, and volcanic glass were observed in the Hul- and Cpt-rich samples in transmitted light (b−d). Abbreviations are given in Table 1.

The Hul/Cpt microcrystals were well developed, with mostly tabular and coffin-shaped intergrowths and rarely acicular. Their dimensions varied from 5 to 15 µm long and from 5 to 10 µm wide (Figure 7a−f). Hul/Cpt was observed with erionite and chabazite in the open cavities of the pumice/tuff (Figure 7a,d,g,h) and replaced glass throughout the zeolitic tuff. Smectite had a typical honeycomb texture and occurred in overgrowths around or between the well-developed Hul/Cpt laths that formed from the pumice (Figure 7e,f,i). Erionite bundles were needle-shaped and fibrous and were located in the cavities of the pumice with chabazite and Hul/Cpt (Figure 7g−h). Chabazite exhibited a pseudocubic habit with well-developed penetration twins. The albite crystals showed comb-like edges and euhedral K-feldspars were observed on the albite. The shapes were interpreted as the dissolution of albite and as the formation of zeolite (*e.g.* clinoptilolite). The subhedral albite crystals may have dissolved at the edges leading to

the comb/finger shapes, probably forming Hul/Cpt (Figure 7i). The neoformed K-feldspar crystals were well developed and had somewhat sharp boundaries that resulted from the progressive dissolution of albite and in the matrix. Corroded, dissolved subhedral quartz crystals were also observed in the samples.

Based on the EDS analysis, the SiO_2 and Al_2O_3 contents of the Hul/Cpt varied from 70.89 to 78.74% and from 15.53 to 22.84% (Table 2), respectively (Figure 7, areas 1, 3−5, 8). The SiO_2/Al_2O_3 ratios of the minerals were between 3.10 and 5.07, suggesting the presence of mostly Ca-rich Hul/Cpt with intermediate to high SiO_2/Al_2O_3 ratios. The monovalent oxides were less abundant than the divalent oxides, and Ca was the most abundant extraframework cation in the minerals, followed by Na. The least abundant cation was K. The EDS analysis suggests that the samples investigated contained both heulandite and clinoptilolite. The SiO_2 and Al_2O_3 contents of the erionites varied from 70.19 to 73.56%
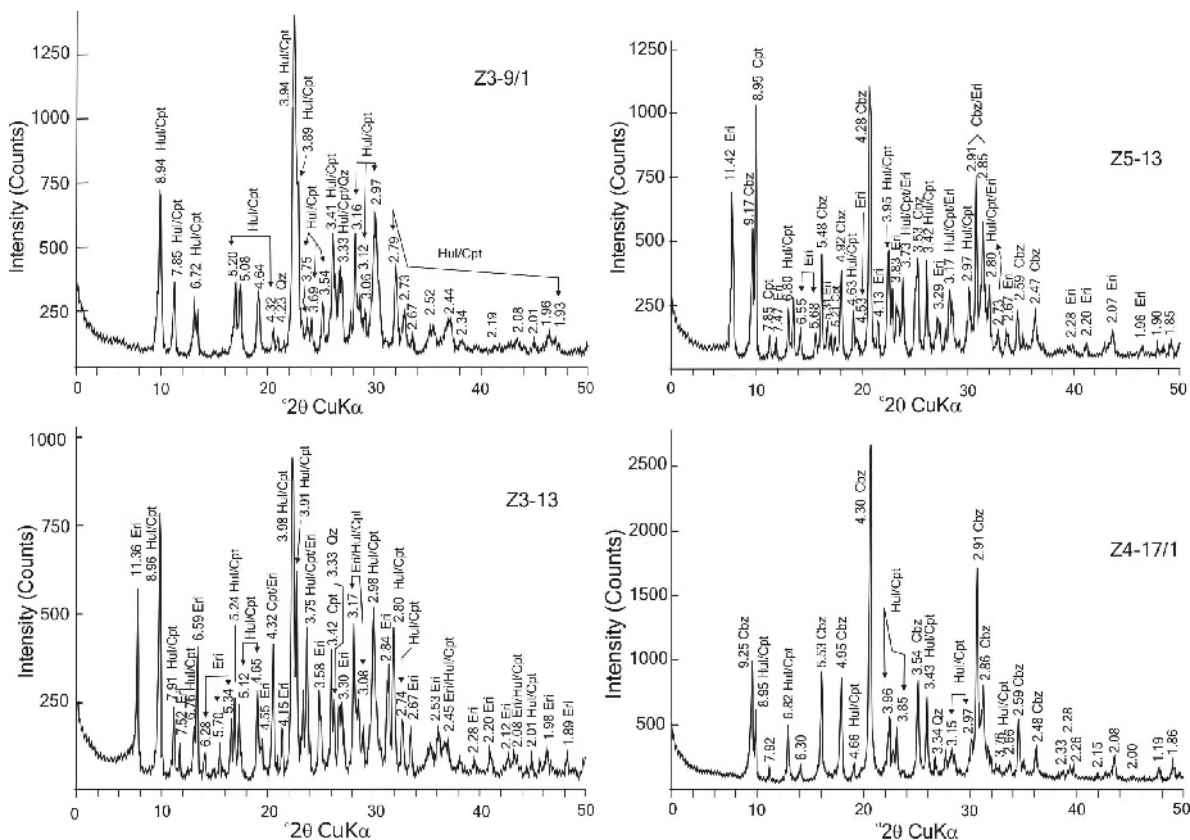
Figure 6. Representative XRD patterns of untreated and air-dried random powder bulk samples of the studied Hul/Cpt-, chabazite-, and erionite-rich samples showing the main reflections (Å) (abbreviations are given in Table 1).

and from 17.76 to 73.56%, respectively. The SiO_2/Al_2O_3 ratio was usually <4.0 (mean of 3.95), and the divalent cations of the erionite, unlike the Hul/Cpt, were usually less abundant their monovalent counterparts. The SiO_2 and Al_2O_3 contents of the chabazite were similar to the erionite, whereas the divalent cations were slightly more abundant and the monovalent cations were less abundant

than in the erionites (Table 2; Figure 7 areas 6, 10). The K_2O and Na_2O contents of the K-feldspar and albite were similar to the theoretical formulae. The samples from area 12 (of Figure 7i) contained a combination of albite and K-feldspar, which may represent an anorthoclase composition (Table 2; Figure 7 areas 11−13). Examination by SEM and analysis by EDS revealed that

Table 2. EDS analysis results (wt.%) of the areas indicated in Figure 7.

Area/Mineral	SiO_2	Al_2O_3	Na_2O	K_2O	MgO	CaO
1. Hul/Cpt	70.89	22.84	–	–	2.96	3.32
2. Eri	73.56	17.76	–	4.22	–	4.46
3. Hul/Cpt	78.74	15.53	–	1.42	0.91	3.40
4. Hul/Cpt	77.29	15.59	–	1.95	0.60	4.57
5. Hul/Cpt	70.32	18.74	4.57	0.93	3.01	2.43
6. Cbz	72.18	18.65	3.50	–	2.29	3.38
7. Eri	72.26	18.20	3.42	2.52	1.99	1.61
8. Hul/Cpt	72.09	18.84	3.10	0.44	2.35	3.18
9. Eri	70.19	18.74	3.93	2.70	2.08	1.54
10. Cbz	72.26	17.89	2.95	1.25	1.94	3.72
11. Kfs	65.30	19.81	4.11	9.20	1.58	–
12. Ab/Kfs	65.23	20.15	4.96	7.86	1.02	0.78
13. Ab	59.60	24.11	11.95	0.69	–	3.65
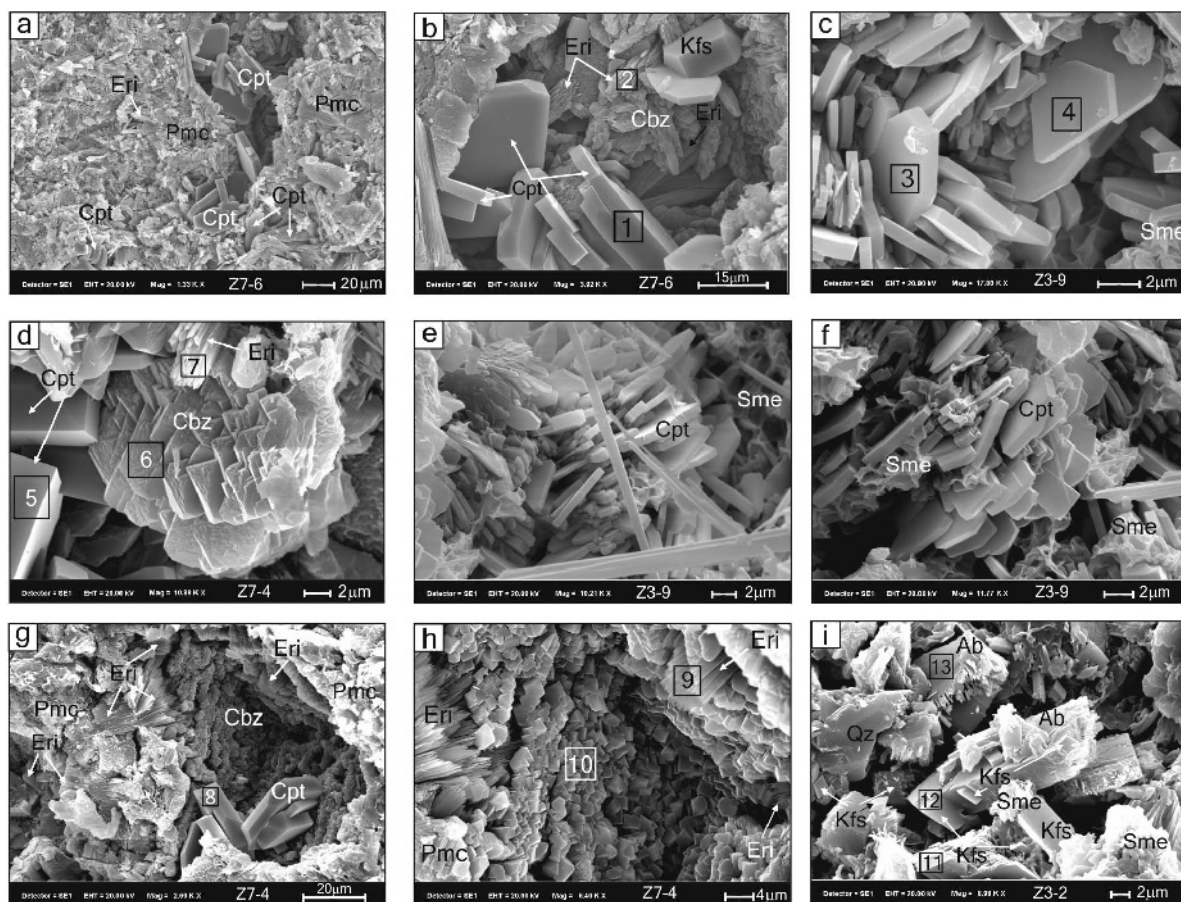
Figure 7. SEM images of zeolites formed from pyroclastic rocks: (a) alteration of pumice primarily to Hul/Cpt and some erionite and chabazite in a cavity; (b) detailed view of (a) showing well developed tabular and coffin-shaped Hul/Cpt crystals. Needle-shaped erionite-like bundles are adjacent to chabazite microcrystals; (c) well developed Hul/Cpt crystals. The Hul/Cpt laths have a characteristic monoclinic symmetry; (d) subhedral chabazite crystals with erionite and Hul/Cpt; (e−f) cornflake-shaped smectite around or between well developed Hul/Cpt laths. The smectite shows a transformation from Hul/Cpt; (g) well developed pseudocubic chabazite and needle-shaped erionite bundles in a cavity in the pumice; (h) detailed view of (g); (i) transformation of albite to zeolite (Hul/Cpt), and the formation of K-feldspar. The subhedral albite crystals have dissolved at the edges and transformed into comb/finger-shaped crystals, probably of Hul/Cpt. Well-developed K-feldspar crystals are present on the albite and in the matrix. A corroded and dissolved subhedral quartz crystal was also observed in the sample (abbreviations listed Table 1).

the K-feldspar was authigenic, formed from the dissolution of albite and/or volcanic glass (Figure 7i).

Geochemistry

The chemical compositions of the Karacadağ volcanics in the study area varied widely (Table 3) (Kurt *et al*., 2008). These volcanic rocks included low- to moderate-silica basalts, hornblende andesites, trachyandesites, and dacites. The alkaline and alkaline earth element contents also varied widely, and the SiO_2, Al_2O_3, and Fe_2O_3 contents of the lavas and weakly altered tuffs were greater than in the zeolitic tuffs (Table 3). The contents of the mono- and divalent cations varied widely in the sections that are rich in zeolite minerals (Table 4). The different chemical compositions of the tuffs played important roles in fluctuations of the element concentrations and mineral

contents in the sections that contained zeolites and other authigenic minerals (Figure 4).

Based on microprobe and thin-section examinations of the fresh lavas and tuffs, the plagioclase minerals consisted mainly of oligoclase and, to a lesser extent, of andesine (Karakaya *et al.*, 2013), which indicated that the volcanics studied were mainly intermediate in composition. The chemical compositions of the (1) zeolite-rich tuffs, (2) zeolite-free tuffs (vitric), and (3) bentonites studied were compared with the precursor volcanic rocks in the area. The immobile elements could be used to distinguish the source rock and indicate the composition of the original volcanic rocks (Rollinson, 1993; Karakaya, 2009; Karakaya *et al.*, 2011, 2012, 2013). The zeolite-rich tuffs plot near the boundary between the trachyte and rhyodacite/dacite fields on the Zr/TiO_2–Nb/Y immobile element ratio diagrams (Winchester and Floyd, 1977), and

Table 3. Chemical compositions of the volcanic rocks and bentonite in the study area.

Sample Element	Basalt $n = 5$	Trachyandesite $n = 7$	Hornblende andesite $n = 14$	Dacite $n = 10$	Bentonite $n = 12$	Tuff $n = 11$	Hul/Cpt $n = 5$	Eri $n = 2$	Cha $n = 2$
SiO_2	50.41	60.63	60.59	64.79	52.78	63.51	63.33	59.70	56.80
Al_2O_3	15.90	17.15	16.23	16.01	11.97	14.70	12.63	17.65	14.04
Fe_2O_3	8.85	5.58	5.76	4.47	5.11	3.29	1.02	2.20	0.48
MgO	6.47	1.51	2.79	1.70	6.32	1.81	1.66	2.00	2.72
CaO	8.97	5.03	6.14	4.96	4.66	4.17	2.71	3.60	1.74
Na_2O	3.56	4.78	3.82	3.80	1.71	2.74	1.30	2.70	2.42
K_2O	1.88	1.87	1.69	1.54	2.43	1.64	1.79	2.40	1.28
TiO_2	1.41	1.00	0.79	0.54	0.64	0.46	0.11	0.15	0.08
P_2O_5	0.60	0.48	0.40	0.27	0.22	0.26	0.03	0.04	0.01
MnO	0.14	0.06	0.09	0.06	0.07	0.04	0.02	0.01	0.01
Cr_2O_3	0.020	0.020	0.020	0.020	0.031	0.010	0.003	0.002	0.002
LOI	1.60	1.74	1.53	1.74	13.81	7.27	14.99	9.00	20.08
Total	99.87	99.84	99.83	99.88	99.77	99.80	99.65	99.70	99.66
Ba	580	598	755	627	327	470	1045	482	1618
Co	34.30	11.99	15.37	10.43	20.16	4.54	1.75	4.55	3.02
Cs	2.78	1.24	1.61	1.80	7.68	4.38	4.77	9.65	1.10
Ga	16.98	17.73	18.04	17.33	13.24	14.56	15.4	17.45	7.9
Hf	3.88	4.14	3.63	3.45	3.10	2.94	4.54	3.40	3.62
Nb	21.78	18.47	13.57	10.01	13.09	7.5	20.7	10.2	13.34
Rb	43.02	40.83	41.8	36.7	108.54	25.96	73.8	76.5	21.78
Sr	874	590	698	564	437	406	1662	1339	1107
Ta	1.32	1.20	0.84	0.69	0.90	0.52	4.24	0.70	1.96
Th	6.28	6.19	8.46	8.35	9.34	6.04	27.83	9.50	32.16
U	1.42	1.76	2.39	2.56	5.18	1.48	5.90	1.40	1.02
V	180.00	103.70	111.90	80.40	98.76	52.60	15.60	78.50	13.00
Zr	152.90	160.69	136.25	119.31	112.79	72.70	91.10	123.00	78.52
Y	24.24	20.13	18.65	15.03	16.64	12.14	28.14	7.45	4.06
La	36.82	32.23	35.10	31.01	21.04	20.42	26.53	31.35	25.84
Ce	68.00	58.64	63.19	53.65	42.29	38.58	52.00	52.85	45.40
Pr	7.90	6.53	6.91	5.68	4.68	3.89	5.94	5.55	4.14
Nd	31.34	24.70	26.34	20.79	17.36	13.88	21.56	17.55	12.32
Sm	5.62	4.51	4.51	3.57	3.26	2.09	4.85	3.05	1.92
Eu	1.68	1.27	1.22	0.98	0.85	0.66	0.36	0.85	0.26
Gd	5.24	3.79	3.88	2.88	3.01	1.87	4.94	2.40	1.42
Tb	0.72	0.58	0.56	0.44	0.50	0.26	0.89	0.30	0.22
Dy	4.22	3.34	3.23	2.51	2.78	1.32	4.86	1.45	0.94
Ho	0.90	0.72	0.60	0.46	0.56	0.26	0.91	0.25	0.16
Er	2.37	1.88	1.74	1.40	1.59	0.75	2.54	0.65	0.36
Tm	0.36	0.29	0.27	0.20	0.25	0.11	0.38	0.10	0.06
Yb	2.19	1.78	1.70	1.44	1.65	0.69	2.48	0.65	0.32
Lu	0.31	0.29	0.26	0.21	0.26	0.11	0.35	0.10	0.06
REE	167.7	140.6	149.5	125.2	100.08	84.88	128.5	117	93.32
LRE	144.1	122.1	131.5	111.1	85.37	76.77	106.1	107.4	87.7
HRE	5.23	4.24	3.97	3.25	3.75	1.65	5.76	1.50	0.76
TRE	613.5	141.9	193.4	138.6	440.4	164.3	63.6	251.5	62.9
LILE	17217	16853	15634	14109	26812	13075	24160	33953	23841
HFSE	11251	8274	6636	4549	2703	2755	699	1210	634
Eu*	1.01	1.00	0.95	1.00	0.88	0.70	0.24	1.03	0.51
Ce*	0.96	0.97	0.98	0.97	1.03	0.99	1.00	0.96	1.06

Volcanic rock values after Kurt *et al.* (2008). Abbreviations are given Table 1.

the zeolite-free tuffs and lavas plot in the trachyandesite field and partly in the andesite field. These results may indicate the compositions of the parent rocks of the zeolitic tuffs (Karakaya *et al.*, 2013).

The SiO_2/Al_2O_3 ratios of the Hul/Cpt-rich samples varied from 4.20 to 5.30 (mean 5.01). The mean SiO_2/Al_2O_3 ratios in the basaltic, trachyandesitic, hornblende andesitic, and dacitic lavas were 3.17, 3.54, 3.73, and

Table 4a. Major (wt.%), trace and rare earth (ppm) elements, and some element and chondrite-normalized ratios from the samples from sections Z0 and Z3.

	Z0-1	Z0-2	Z0-3	Z0-4	Z0-5	Z3-1	Z3-2	Z3-4	Z3-5	Z3-6	Z3-7	Z3-8	Z3-9	Z3-10	Z3-11	Z3-12	Z3-13	Z3-14	MDL	STD*
SiO_2	59.90	59.50	57.30	63.50	64.30	64.70	46.91	47.18	59.10	52.80	60.80	55.41	62.90	52.82	49.94	48.88	63.90	64.30	0.01	58.04
Al_2O_3	17.40	17.90	14.10	11.70	13.40	12.20	8.93	8.35	13.70	9.80	13.20	11.56	13.40	9.77	10.24	10.98	12.90	12.30	0.01	14.14
Fe_2O_3	2.30	2.10	4.40	1.30	1.40	0.90	3.59	3.04	0.80	3.60	1.50	3.85	0.50	3.92	3.80	4.44	0.70	1.20	0.04	7.61
MgO	2.20	1.80	4.10	2.10	1.30	1.40	11.05	10.00	3.10	10.33	5.00	8.04	1.70	10.43	8.56	7.18	1.70	1.40	0.01	3.33
CaO	3.30	3.90	1.80	4.30	3.00	2.20	6.87	9.30	1.70	3.75	1.10	3.60	1.90	3.64	5.86	6.96	2.60	1.80	0.01	6.38
Na_2O	2.80	2.60	0.90	1.00	1.30	2.00	1.77	1.86	3.10	1.98	2.10	1.75	2.00	2.00	1.89	2.19	1.20	2.30	0.01	3.68
K_2O	2.40	2.40	4.90	2.30	3.50	1.90	1.68	1.49	2.10	1.59	2.40	1.81	2.40	1.80	2.64	2.78	2.20	2.10	0.01	2.16
TiO_2	0.60	0.50	0.60	0.20	0.10	0.10	0.46	0.37	0.10	0.43	0.10	0.44	0.10	0.51	0.47	0.51	0.00	0.10	0.01	0.69
P_2O_5	0.10	0.08	0.04	0.03	0.02	0.07	0.07	0.20	0.00	0.12	0.02	0.08	0.03	0.06	0.31	0.09	0.01	0.02	0.01	0.82
MnO	0.01	<0.01	0.10	0.00	0.00	<0.01	0.15	0.08	<0.01	0.05	0.1	0.04	0.01	0.07	0.07	0.09	<0.01	<0.01	0.01	0.39
Cr_2O_3	0.027	0.009	0.031	0.00	<0.002	<0.002	0.019	0.017	<0.002	0.015	<0.002	0.041	<0.002	0.021	0.021	0.018	<0.002	<0.002	0.00	0.55
LOI	8.80	9.20	11.50	13.20	11.50	14.4	18.1	17.8	16.1	15.3	13.7	13.1	14.9	14.7	15.9	15.6	14.4	14.2	5.10	25.00
SUM	99.70	99.70	99.70	99.70	99.70	99.8	99.64	99.72	99.8	99.74	99.9	99.76	99.8	99.74	99.69	99.72	99.8	99.8		1.90
TOT/C	0.10	0.10	0.20	0.70	0.20	0.1	3.08	2.17	0.2	0.92	0	0.83	0.1	1.38	1.52	1.7	0.0	0.0	0.01	99.70
TOT/S	0.10	0.10	<0.02	<0.02	<0.02	<0.02	0.03	0.16	<0.02	0.04	<0.02	0.03	<0.02	<0.02	0.04	0.06	<0.02	<0.02	0.02	497.0
Ba	469	494	338	383	3090	319	264	320	768	227	75	328	196	201	638	609	382	280	0.02	27.20
Sc	10.0	6.0	11.0	9.0	3.0	3.0	9.0	8.0	2.0	19.0	8.0	9.0	3.0	10.0	9.0	11.0	3.0	5.0	0.02	6.90
Co	5.10	4.00	23.20	4.20	2.10	1.3	12.7	12	4.6	13.8	2.3	15.1	3.3	13.5	14.3	16.5	2.2	<0.2	0.02	17.20
Cs	31.6	27.7	31.7	18.4	8.7	3.3	11	6.4	2.7	12.9	20.6	6.0	3.3	12.6	6.8	9.9	2.6	2.7	1.00	9.60
Ga	18.5	16.4	17.4	17.8	18.9	16.9	10.2	8.6	6.6	11.6	18	14.1	18.2	10.2	11.6	12.2	16.9	18.6	0.20	21.20
Hf	3.4	3.4	3.5	3.1	2.9	4.1	2.2	2.2	2.6	2.5	3.5	2.9	4.5	2.7	2.8	2.6	5.7	4.0	0.10	28.20
Nb	12.1	8.3	17.4	44.0	16.8	36.1	9.7	9.1	2.6	13.4	43.1	13.7	20.5	10.4	9.9	10.3	31.2	38.8	0.50	15.00
Rb	76.0	77.0	168.0	112.0	117.0	67.2	92.7	85.6	74.9	102.6	189	91.1	80.5	94.1	131.5	129.6	86.3	71.7	0.10	406.80
Sr	1244	1434	1114	1862	2431	1239	1003	474.5	931	316	120	446	1017	376	583	495	876	825	0.10	720.00
Ta	0.7	0.7	1.3	4.4	7.6	5.9	0.6	0.7	1.6	1.1	8.2	0.7	6.9	0.7	0.7	0.7	7.7	6.2	0.10	10.30
Th	9.4	9.6	10.7	27.5	13.6	31.2	11.3	7.9	14.3	9.4	32.4	5.4	29.7	8.1	7.3	8.4	25.9	38.9	0.10	16.40
U	1.6	1.2	0.8	1.5	2.3	12.1	11.7	6.1	0.4	8.7	8.4	3.5	5.4	14.1	17.0	4.4	3.4	14.4	0.10	207.00
V	77.0	80.0	100.0	36.0	14.0	12.0	76.0	57.0	16.0	127.0	9.0	62.0	<8	86.0	80.0	103.0	<8	9.0	0.10	14.80
W	0.7	0.6	1.3	8.4	<0.5	2.8	4.0	3.2	5.8	3.1	12.6	5.2	5.1	4.0	4.7	4.3	5.8	<0.5	0.20	19.10
Zr	135.0	111.0	142.0	96.4	54.1	74.4	88.7	82.2	43	87.9	63.2	97.8	73	102.5	95.9	91.5	103	74.4	0.10	106.9
Y	7.7	7.2	17.1	16.7	12.1	23.5	27.9	10.7	2	12.8	23.6	8.9	46.5	16.4	12.6	12.9	20.3	81.4	0.10	65.90
La	34.7	28.0	37.3	18.0	13.3	15	15.4	12.8	6.1	15.1	15.6	14.7	14.3	14.9	17.2	19.7	11.9	19.2	0.10	385.0
Ce	57.7	48.0	80.3	36.0	28.4	33	29.7	26	12.6	30.1	34.5	26.7	30.7	30	34.3	38.5	26.9	35.2	0.10	53.20
Pr	6.5	4.6	7.1	4.2	3.1	4	3.35	2.82	1.3	3.31	4.1	3.16	3.7	3.3	3.7	4.21	3.2	6.6	0.02	53.80
Nd	20.9	14.2	25.8	14.6	11.9	14.8	12	10.5	4.1	12.1	14.3	11.8	14.3	12.1	13.8	15.5	11.6	27.2	0.30	5.80
Sm	3.7	2.4	4.3	3.9	3.2	4.3	2.4	1.97	0.8	2.3	4.9	2.01	4.7	2.25	2.55	2.86	3.4	8.9	0.05	3.30
Eu	1.0	0.7	1.0	0.3	0.1	0.1	0.59	0.47	0.1	0.54	0.1	0.55	0.1	0.58	0.66	0.71	0.1	0.2	0.02	4.40
Gd	2.7	2.1	4.1	3.8	3.1	4.2	2.41	1.86	0.6	2.25	5.2	1.73	5.7	2.04	2.26	2.55	3.4	11.3	0.05	0.70
Tb	0.3	0.3	0.6	0.7	0.5	0.8	0.44	0.32	0.1	0.4	1.0	0.26	1.2	0.35	0.38	0.41	0.6	2.4	0.01	51.00
Dy	1.6	1.3	3.2	3.4	2.3	4	2.93	1.69	0.4	2.16	4.6	1.33	7.1	2.16	2.1	2.24	3.4	13.6	0.05	0.20
Ho	0.3	0.2	0.6	0.6	0.4	0.7	0.73	0.35	0.1	0.42	0.8	0.28	1.5	0.49	0.43	0.44	0.6	2.7	0.02	4.30
Er	0.7	0.6	1.7	1.3	1.1	1.9	2.6	1.0	0.2	1.14	1.8	0.78	4.2	1.61	1.18	1.26	1.7	7.7	0.03	3.70

	Z4-1	Z4-2	Z4-3	Z4-5	Z4-6	Z4-7	Z4-8	Z4-9	Z4-10	Z4-11	Z4-12	Z4-14	Z4-15	Z4-16	Z4-17/1	MDL	STD
Tm	0.1	0.1	0.2	0.2	0.3	0.48	0.0	0.18	0.3	0.12	0.31	0.18	0.19	0.3	1.1	0.01	284.9
Yb	0.7	0.6	1.6	1.0	2.0	3.67	0.2	1.23	1.7	0.86	2.55	1.19	1.2	1.8	7.3	0.05	31.50
Lu	0.1	0.1	0.2	0.2	0.3	0.63	0.0	0.18	0.2	0.13	0.44	0.19	0.18	0.3	1.0	0.01	12.10
Cu	11.0	6.2	20.4	12.9	1.2	18.8	1.6	18.3	1.5	52.8	22.4	25.7	25.7	0.9	2.0	0.02	27.30
Pb	7.4	11.2	21.3	35.4	30.7	9.6	34.8	14.9	38.2	8.2	10.9	12.6	15.4	42.4	71.8	0.02	3.41
Zn	15.0	9.0	25.0	24.0	38.0	35.0	24.0	43.0	34.0	41.0	42.0	41.0	49.0	32.0	37.0	0.20	13.90
Ni	22.0	11.7	180.0	28.3	3.0	63.9	10.1	76.4	3.9	177.1	72.7	83.0	85.3	1.5	2.0	0.10	2.91
As	39.4	54.9	29.3	3.5	11.1	35.6	5.4	110.3	3.5	23.6	26.0	32.9	69.8	1.7	37.4	0.20	0.86
REE	131.0	103.2	168.0	88.4	85.4	77.3	26.6	71.4	89.1	64.4	73.1	80.1	90.0	69.2	144.4		
LREE	123.5	97.2	154.8	76.7	71.1	62.9	24.9	62.9	73.4	58.4	62.6	71.6	80.8	57.0	97.1		
MREE	5.90	4.60	9.50	8.80	9.80	7.10	1.30	5.77	11.70	4.15	5.62	5.83	6.35	8.10	30.20		
HREE	1.60	1.40	3.70	2.90	4.50	7.38	0.40	2.73	4.00	1.89	4.91	2.74	2.83	4.10	17.10		
TRE	324.8	178.5	571.7	127.4	58.5	345.4	58.3	400.1	58.7	637.5	390.3	396.7	413.7	39.6	55.0		
LILE	21823	22027	42448	34810	17520	15384	19275	13923	20437	15950	15692	23357	24398	19718	18789		
HFSE	4185	3470	3936	768	1026	3164	737	3206	848	3102	3436	4280	3555	191	810		
Eu*	0.96	0.95	0.73	0.24	0.07	0.75	0.51	0.72	0.06	0.90	0.83	0.84	0.80	0.09	0.06		
Ce*	0.93	1.02	1.19	1.00	1.03	1.00	1.08	1.03	1.04	0.95	1.04	1.04	1.02	1.05	0.76		
LR/HR	77.2	69.4	41.8	26.4	15.8	8.5	62.3	23.0	18.4	30.9	12.7	26.1	28.5	13.9	5.7		

Note: MDL: Method Detection Limit; STD*: the in-house standards used by ACME Laboratories for major and trace, and refractory elements (known as SO-18 and DS7).

Table 4b. Major (wt.%), trace, and rare earth (ppm) elements, and some element and chondrite-normalized ratios from the samples from section Z4.

	Z4-1	Z4-2	Z4-3	Z4-5	Z4-6	Z4-7	Z4-8	Z4-9	Z4-10	Z4-11	Z4-12	Z4-14	Z4-15	Z4-16	Z4-17/1	Z4-17/2
SiO_2	56.65	51.86	52.03	59.25	54.93	60.47	61.30	50.70	56.54	58.32	57.20	59.70	57.02	54.13	57.70	57.40
Al_2O_3	14.92	11.99	11.03	13.66	11.35	14.04	12.75	13.29	14.63	11.68	14.10	13.20	13.94	11.72	13.50	13.60
Fe_2O_3	2.88	4.68	4.53	0.38	4.80	1.21	5.15	5.85	0.34	5.20	0.40	1.00	0.76	4.88	0.30	0.60
MgO	2.52	5.43	3.64	1.85	4.68	2.34	4.49	5.97	2.23	4.22	2.50	3.20	2.93	4.49	2.90	3.40
CaO	0.58	7.03	8.11	1.37	6.85	1.57	2.09	3.54	2.38	4.36	2.60	2.50	1.88	6.38	1.10	1.30
Na_2O	4.53	2.72	1.91	3.66	2.09	3.64	1.89	0.69	1.89	1.82	1.20	0.90	2.74	1.70	2.60	2.00
K_2O	2.49	2.16	2.37	1.23	2.21	1.86	2.32	2.35	1.49	2.19	1.30	1.10	1.25	2.33	1.10	1.10
TiO_2	0.26	0.72	0.76	0.04	0.79	0.20	0.76	0.64	0.07	0.79	0.10	0.10	0.07	0.67	0.10	0.10
P_2O_5	0.08	0.18	0.45	0.01	0.19	0.05	0.16	0.69	0.02	0.14	<0.002	<0.002	0.03	0.31	0.00	0.00
MnO	0.03	0.09	0.19	<0.01	0.10	<0.01	0.05	0.07	<0.01	0.08	<0.01	<0.01	<0.01	0.12	<0.01	<0.01
Cr_2O_3	0.004	0.03	0.03	<0.002	0.04	0.01	0.06	0.03	<0.002	0.05	<0.002	<0.002	<0.002	0.04	<0.002	<0.002
LOI	15.0	12.9	14.8	17.9	11.7	14.2	8.8	15.9	20.0	10.9	20.3	17.5	19.2	13.0	20.4	20.3
Sum	99.9	99.8	99.8	99.4	99.8	99.6	99.8	99.8	99.6	99.8	99.6	99.1	99.8	99.8	99.7	99.8
TOT/C	0.1	1.5	1.7	0.03	1.43	0.1	0.25	0.55	<0.02	0.81	<0.02	0.03	<0.02	1.28	0.1	0.01
TOT/S	<0.02	0.3	0.24	0.07	0.06	0.1	<0.02	<0.02	<0.02	<0.02	<0.02	<0.02	<0.02	0.03	0.1	0.01
Ba	102	280	249	3643	317	1724	299	235	1887	446	1510	5014	617	410	1600	831
Sc	3.0	5.0	6.0	<1	11.0	3.0	12.0	13.0	<1	12.0	1.0	1.0	<1	10	1.0	1.0
Co	6.9	<0.2	19.9	1.9	18.9	7.2	25.9	24.6	2.5	23	2.7	4.3	4.8	22.2	1.0	2.9
Cs	1.5	2.7	5.0	0.7	4.3	1.6	4.8	7	1.2	4.7	1.5	1.1	1.1	4.3	0.8	1.2
Ga	13.7	18.6	12.1	6.2	11.7	10.5	12.9	16.4	6.7	15.1	6.8	10.4	11.4	12.3	4.9	7.6

Table 4b (*contd.*)

	Z4-1	Z4-2	Z4-3	Z4-5	Z4-6	Z4-7	Z4-8	Z4-9	Z4-10	Z4-11	Z4-12	Z4-14	Z4-15	Z4-16	Z4-17/1	Z4-17/2
Hf	3.0	4.0	3.0	3.0	3.7	3.0	4.2	3.4	4.1	3.8	4.2	3.1	3.1	3.0	3.8	3.6
Nb	10	38.8	14.1	6.0	14.4	9.2	13.3	16.5	13.2	15.5	17.2	11.6	11.8	12.1	21.9	10.6
Rb	48	71.7	87.2	21.9	77.9	41.1	92.1	110	25	78.6	22.9	26.9	21.8	81	17.8	24.3
Sr	213	825	393	1551	424	1158	296	433	1346	321	1224	2763	936	544	973.4	799.1
Ta	1.2	6.2	1.0	1.7	1.0	1.6	0.9	1.1	2.2	1.0	2.3	1.9	1.9	0.8	2.0	1.8
Th	10	38.9	10.4	34.9	8.5	18.9	8.6	15.8	45.4	8.6	50.2	22.4	17.8	8.9	41.2	37.8
U	1.4	14.4	2.0	0.9	2.7	0.8	1.8	11.4	1.3	2.5	1.7	0.4	0.5	6.2	1.2	1.6
V	27	9	82	<8	82	20	87	101	11	93	<8	<8	<8	93	13	15
W	<0.5	<0.5	2.5	4.6	7.8	14.5	12.5	2.5	3.9	1.8	3.6	6.7	3.8	1.4	<0.5	3.3
Zr	86	74.4	119	66.1	138	72.6	148	115	84.6	157	79.7	87.7	76.5	116	63.5	80.1
Y	9.2	81.4	17.5	4.5	19.5	6.3	18.2	20.3	5.4	22.6	6.5	3.3	2.5	17.3	5.1	5.4
La	29.3	22.7	22.8	22.0	24.6	23.9	23.0	27.5	22.7	24.1	32.4	27.5	33.3	22.7	32.4	15.4
Ce	55.1	47.4	48.2	38.3	48.8	43.8	46.7	50.7	46.0	51.5	56.2	50.7	57.9	46.0	56.2	28.6
Pr	5.6	5.1	5.0	3.6	5.7	4.0	5.3	5.5	5.0	5.6	5.4	5.5	5.4	5.0	5.4	2.8
Nd	18.2	17.6	18.4	10.5	21.3	12.6	19.6	20.5	19.0	22.4	15.5	20.5	16.3	19.0	15.5	8.6
Sm	2.7	3.6	3.4	1.7	4.1	2.1	3.7	3.6	3.5	4.0	2.6	3.6	2.5	3.5	2.6	1.5
Eu	0.7	1.0	0.9	0.2	1.1	0.4	1.0	0.9	0.9	1.1	0.3	0.9	0.3	0.9	0.3	0.2
Gd	2.1	3.5	3.3	1.3	3.7	1.6	3.4	3.3	3.4	4.1	2.1	3.3	1.7	3.4	2.1	1.1
Tb	0.3	0.6	0.5	0.2	0.6	0.2	0.6	0.6	0.5	0.7	0.3	0.6	0.3	0.5	0.3	0.2
Dy	1.5	3.0	2.8	0.9	3.3	1.2	3.1	3.1	2.8	3.8	1.6	3.1	1.1	2.8	1.6	0.7
Ho	0.3	0.6	0.6	0.2	0.7	0.2	0.6	0.7	0.6	0.8	0.3	0.7	0.2	0.6	0.3	0.1
Er	0.8	1.7	1.7	0.4	1.8	0.5	1.8	1.8	1.7	2.5	0.6	1.8	0.5	1.7	0.6	0.2
Tm	0.1	0.3	0.2	0.1	0.3	0.1	0.3	0.3	0.2	0.4	0.1	0.3	0.1	0.2	0.1	0.0
Yb	0.7	1.6	1.6	0.4	1.8	0.5	1.7	2.0	1.7	2.4	0.5	2.0	0.4	1.7	0.5	0.2
Lu	0.1	0.2	0.3	0.1	0.3	0.1	0.3	0.3	0.3	0.4	0.1	0.3	0.1	0.3	0.1	0.0
Cu	11.0	2.0	26.6	2.0	24.3	7.2	27.1	33.7	3.0	23.5	2.1	4.6	5.6	24.2	1.3	2.3
Pb	178.0	71.8	15.0	20.2	13.1	38.0	15.2	31.3	13.5	12.4	20.9	25.9	36.9	13.2	23.7	33.4
Zn	510	37	47	21	54	25	57	77	9	59	22	30	27	50	21	26
Ni	28.0	2.0	107.0	4.4	130.0	27.0	132.5	148.6	7.4	143.4	3.5	8.0	10.3	114.9	4.9	7.9
As	9.1	37.4	2.1	4.1	10.3	11.5	11.8	10.1	1.4	7.6	1.7	2.0	4.2	20.9	2.6	2.6
REE	117.4	108.8	109.6	79.7	118.1	91.2	111.0	120.7	108.3	123.6	118.0	120.7	119.9	108.3	117.8	59.7
LREE	108.2	92.8	94.4	74.4	100.4	84.3	94.6	104.2	92.7	103.6	109.5	104.2	112.9	92.7	109.5	55.4
MRE	7.54	12.26	11.41	4.40	13.47	5.70	12.43	12.07	11.78	14.44	7.20	12.07	6.05	11.78	7.09	3.70
HRE	1.75	3.74	3.76	0.86	4.20	1.20	3.96	4.39	3.82	5.60	1.30	4.39	0.97	3.82	1.20	0.54
TRE	613.3	260.3	500.6	29.3	614.4	164.7	731.5	575.8	32.9	696.0	31.3	65.7	47.7	581.1	42.2	55.1
LILE	2712	3150	2795	6354	2751	4593	2708	2865	4655	2763	3997	8844	2759	3066	3654	2715
HFSE	3249	4059	4896	6474	3737	4897	3573	6013	6112	3551	4101	8948	2983	4551	3745	2811
Eu*	0.93	0.87	0.90	0.48	0.90	0.71	0.92	0.83	0.88	0.88	0.42	0.83	0.41	0.88	0.42	0.49
Ce*	1.04	1.06	1.08	1.04	0.99	1.08	1.02	0.99	1.04	1.07	1.02	0.99	1.04	1.04	1.02	1.04
LR/HR	61.8	24.8	25.1	86.5	23.9	70.3	23.9	23.7	24.3	18.5	84.2	23.7	116.4	24.3	91.3	102.7

Table 4c. Major (wt.%), trace, and rare earth (ppm) elements, and some element and chondrite-normalized ratios from samples from section Z5, Hul/Cpt-rich samples, and lava samples.

Samples Elem.	Z5 Section samples															Hul/Cpt-rich samples			Lava samples			
	Z5-2	ZZ-3	Z5-4	Z5-5	Z5-6	Z5-10	Z5-9	Z5-7	Z5-16	Z5-15	Z5-14	Z5-13	Z5-12	Z5-11	Z5-17	Z13-2	Z16-7	Z19-5	Z12-2	Z12-3	Z12-7	Z16-1
SiO_2	63.1	54.8	49.1	52.1	17.7	52.0	49.6	58.1	53.8	51.2	55.4	58.1	52.1	58.4	53.9	61.10	64.40	62.03	72.23	70.91	68.94	65.45
Al_2O_3	13.1	13.6	11.7	9.7	3.5	13.8	13.1	13.8	12.1	13.1	14.6	13.8	12.1	13.3	12.7	13.90	11.40	12.34	14.00	13.45	15.89	15.32
$Fe2O3$	0.8	4.4	4.8	3.7	1.4	6.9	7.1	0.5	5.9	6.7	0.4	0.8	5.8	1.2	5.1	0.30	1.75	1.79	2.35	2.39	2.89	3.68
MgO	1.7	5.3	5.7	7.5	16.3	5.7	5.3	1.6	4.8	6.1	2.2	2.5	6.0	3.2	4.5	1.90	2.05	1.44	0.41	0.96	0.40	1.67
CaO	1.9	2.4	6.6	5.9	22.6	2.8	4.4	1.9	5.3	3.2	2.0	2.2	5.6	1.8	6.2	4.20	3.41	2.85	3.65	3.55	3.92	3.71
Na_2O	2.0	1.1	2.3	1.5	0.7	1.7	1.4	3.6	1.4	1.1	2.9	1.8	1.4	2.7	2.6	0.60	0.27	0.73	3.11	2.90	3.81	3.61
K_2O	2.4	4.2	2.5	1.8	0.5	2.4	2.0	1.4	2.3	3.0	1.4	1.5	2.6	2.0	2.7	0.30	0.96	2.66	1.38	1.40	1.53	1.75
TiO_2	0.1	0.5	0.5	0.5	0.2	0.8	0.7	0.1	0.8	0.9	0.0	0.1	0.8	0.1	0.7	0.10	0.21	0.03	0.29	0.25	0.35	0.46
P_2O_5	0.0	0.1	0.1	0.2	0.1	0.1	0.2	0.02	0.1	0.2	0.02	0.02	0.2	0.1	0.7	0.10	0.04	0.03	0.11	0.11	0.14	0.30
MnO	0.0	0.03	0.1	0.1	0.1	0.1	0.1	0.1	0.1	<0.01	<0.01	0.1	0.0	0.1	<0.01	0.02	0.01	0.01	0.02	0.03	0.01	
Cr_2O_3	<0.002	0.02	0.02	0.02	0.01	0.031	0.032	<0.002	0.08	0.07	<0.002	<0.002	0.09	<0.002	0.09	<0.002	<0.002	0.003	0.01	0.03	0.01	0.00
LOI	14.8	13.5	16.5	16.9	36.6	13.5	15.9	18.7	13.2	14.3	20.5	18.7	13.2	16.8	10.6	16.50	15.20	15.3	2.40	4.00	2.00	3.80
SUM	99.8	99.8	99.7	99.7	99.5	99.8	99.8	99.6	99.8	99.8	99.4	99.5	99.8	99.4	99.8	98.90	99.70	99.74	99.8	99.9	99.9	99.8
TOT/C	0.1	0.7	1.6	2.0	9.0	0.6	1.1	0.1	1.2	0.9	<0.02	<0.02	1.2	0.1	1.0	0.10	0.04	0.08	0.02	0.03	0.03	0.11
TOT/S	<0.02	<0.02	<0.02	<0.02	<0.02	0.4	0.2	<0.02	0.1	<0.02	0.0	<0.02	<0.02	0.4	0.1	<0.02	<0.02	<0.02	<0.02	<0.02	<0.02	<0.02
Ba	196	202	520	326	229	203	270	1853	282	238	3153	2460	244	2844	336	4751	1121	265	340	367	452	752
Sc	2.0	16.0	9.0	11.0	3.0	16.0	17.0	14.0	16.0	14.0	1.0	13.0	2.00	5.00	2.00	3.0	3.0	4.0	4.0	5.0	5.2	6.6
Co	0.6	10.8	16.0	10.4	5.1	27.5	23.0	2.5	31.4	29.9	3.9	2.5	20.4	1.8	19.0	0.30	2.70	0.70	2.5	0.3	0.6	0.2
Cs	3.4	9.7	15.0	5.7	1.3	7.7	6.0	0.8	5.4	8.0	1.2	0.8	5.4	0.8	4.7	2.70	6.70	12.10	0.3	2.2	3.0	3.4
Ga	19.0	14.1	12.9	11.1	4.4	15.9	14.9	12.1	13.0	15.3	8.9	11.7	13.3	12.2	12.7	11.50	12.40	13.40	13.8	13.2	15.0	15.7
Hf	5.1	3.1	2.7	2.7	0.8	3.0	2.7	3.4	3.5	3.4	3.5	3.9	3.1	3.1	3.4	6.00	4.60	2.90	2.4	4.6	7.9	12.3
Nb	18.2	12.0	10.7	11.4	3.7	15.4	14.1	17.5	13.7	16.4	9.2	16.5	13.7	15.2	12.6	1.60	12.10	4.40	5.0	23.5	27.5	34.6
Rb	75.6	172.4	115.2	87.4	19.3	121.0	101.6	22.9	90.6	140.4	20.0	27.3	99.4	43.2	94.3	14.80	46.30	149.7	18.4			
Sr	1055	321	632	610	1390	322	433	1173	306	353	1481	1804	375	1910	773	4756	1151	1770	351	333	394	603
Ta	7.3	1.0	0.7	0.6	0.2	1.0	1.0	2.0	1.0	1.2	1.9	1.9	0.9	1.9	0.8	0.70	1.20	1.10	0.3	0.4	0.6	0.8
Th	36.7	9.9	8.3	7.5	2.5	12.5	9.1	32.1	8.7	12.2	18.6	27.4	9.4	22.5	8.2	41.50	18.50	9.10	4.2	4.3	6.9	8.5
U	5.5	1.5	1.7	2.5	0.7	1.6	1.5	0.5	2.0	1.8	0.5	0.4	4.3	1.5	3.9	4.10	1.00	0.90	0.6	1.0	1.9	2.1
V	63.0	97.0	99.0	32.0	160.0	123.0	113.0	117.0	96.0	89.0	14.00	30.00	13.00	57.0	53.0	43.0	63.0	145.9				
W	3.1	3.3	3.6	5.8	3.9	4.6	4.6	8.3	3.8	3.9	3.7	5.4	8.1	0.50	91.6	75.2	119.6					
Zr	72.0	113.3	99.2	95.5	31.8	108.2	109.1	71.8	122.1	122.7	87.9	89.1	121.2	79.4	128.3	94.00	133.0	85.90				
Y	48.7	16.7	13.2	13.4	6.1	18.8	17.3	6.2	19.8	21.3	1.9	4.1	17.0	6.7	19.9	12.30	7.60	5.40	5.2	5.7	8.2	12.6
La	15.9	18.7	17.8	17.8	7.2	22.7	21.1	28.6	25.1	26.4	25.4	25.5	22.1	17.2	24.3	66.50	33.00	25.70	14.2	13.3	21.6	36.1
Ce	36.5	38.0	37.1	36.1	14.3	47.9	43.4	52.9	50.9	52.5	40.8	44.6	45.5	32.7	51.9	131.2	60.90	46.10	25.7	25.2	39.9	70.5
Pr	4.33	4.10	3.98	3.85	1.54	5.3	4.9	4.7	5.7	5.9	3.3	4.2	5.0	3.3	5.5	13.40	5.74	4.92	2.5	2.54	4.10	7.1
Nd	17.9	15.7	14.3	13.6	5.8	18.3	18.2	14.2	22.4	22.7	8.9	13.0	18.3	10.6	19.6	47.10	20.00	15.90	8.4	9.3	14.4	25.80
Sm	5.49	2.88	2.62	2.64	1.08	3.7	3.4	2.4	4.3	4.2	1.1	2.1	3.7	2.0	3.9	6.50	3.36	2.81	1.5	1.51	2.17	3.4
Eu	0.14	0.71	0.68	0.67	0.28	1.0	0.9	0.3	1.1	1.1	0.1	0.2	0.9	0.3	1.1	1.10	0.42	0.52	0.6	0.57	0.70	0.92
Gd	7.33	2.80	2.43	2.41	1.00	3.5	3.1	1.7	3.9	3.9	0.7	1.5	3.3	1.6	3.7	5.10	2.67	2.21	1.3	1.36	1.95	2.99
Tb	1.38	0.47	0.40	0.41	0.18	0.6	0.5	0.3	0.6	0.6	0.1	0.2	0.5	0.2	0.6	0.60	0.35	0.28	0.2	0.19	0.28	0.40
Dy	8.16	2.72	2.23	2.35	0.91	3.3	3.0	1.3	3.5	3.6	0.4	0.9	3.1	1.2	3.4	2.80	1.72	1.41	1.0	0.88	1.43	2.00
Ho	1.62	0.56	0.44	0.47	0.19	0.6	0.6	0.2	0.7	0.7	0.1	0.1	0.6	0.2	0.7	0.40	0.27	0.17	0.2	0.18	0.27	0.40
Er	4.66	1.58	1.24	1.29	0.54	1.9	1.7	0.5	1.9	2.1	0.1	0.3	1.7	0.6	2.0	1.10	0.75	0.41	0.5	0.53	0.76	1.24
Tm	0.67	0.24	0.20	0.20	0.09	0.3	0.3	0.1	0.3	0.3	0.0	0.0	0.3	0.1	0.3	0.10	0.12	0.06	0.1	0.08	0.11	0.17

Table 4c (contd.)

Elem.	Z5-2	ZZ-3	Z5-4	Z5-5	Z5-6	Z5-10	Z5-9	Z5-7	Z5-16	Z5-15	Z5-14	Z5-13	Z5-12	Z5-11	Z5-17	Z13-2	Z16-7	Z19-5	Z12-2	Z12-3	Z12-7	Z16-1
Samples					Z5 Section samples											Hul/Cpt-rich samples				Lava samples		
Yb	4.71	1.49	1.28	1.19	0.57	1.9	1.7	0.4	1.8	2.0	0.1	0.2	1.8	0.6	2.0	0.80	0.78	0.36	0.1	0.51	0.71	0.18
Lu	0.64	0.23	0.19	0.19	0.09	0.3	0.3	0.0	0.3	0.3	0.0	0.0	0.3	0.1	0.3	0.10	0.11	0.04	10.1	0.07	0.12	8.60
Cu	1.9	18.2	22.6	20.5	4.3	39.9	30.4	1.3	39.2	38.8	3.3	1.6	32.2	4.8	25.3	1.20	8.90	5.10	0.5	0.6	0.9	1.5
Pb	116.8	14.8	17.5	11.7	3.1	20.1	12.2	51.2	18.7	20.2	34.3	50.0	16.2	45.3	13.9	6.30	27.50	18.10	6.8	2.3	2.3	3.2
Zn	10.0	26.0	45.0	38.0	12.0	70.0	63.0	31.0	66.0	85.0	25.0	28.0	66.0	31.0	54.0	7.00	34.00	11.00	1.6	0.5	0.3	0.4
Ni	0.9	49.2	83.7	74.6	23.8	167.2	142.2	7.2	169.9	188.9	9.4	4.3	147.5	7.8	115.7	7.10	9.10	5.70	1.4	1.4	1.7	2.1
As	14.5	38.6	81.3	24.3	10.6	21.3	4.8	17.9	7.0	2.7	4.1	5.7	59.9	12.2	38.0	2.80	2.20	514.0	0.6	1.2	0.8	0.8
REE	109.4	90.2	84.9	83.2	33.8	111.0	103.0	107.6	122.5	126.4	81.2	92.9	107.1	70.6	119.2	276.8	130.3	100.9	52.5	51.8	75.9	124.8
LREE	74.6	76.5	73.2	71.4	28.8	94.2	87.6	100.4	104.1	107.5	78.4	87.3	90.9	63.8	101.3	258.2	119.7	92.6	38.1	38.5	60.6	106.8
MRE	24.12	10.14	8.80	8.95	3.64	12.60	11.51	6.20	14.04	14.13	2.43	5.00	12.13	5.50	13.37	16.50	8.79	7.40	3.67	3.71	5.39	7.95
HRE	10.68	3.54	2.91	2.87	1.29	4.29	3.92	1.00	4.32	4.74	0.31	0.60	4.00	1.34	4.52	2.10	1.76	0.87	10.69	9.56	9.94	10.00
TRE	15.4	313.2	389.6	363.0	134.9	692.7	617.5	42.0	980.9	954.5	41.6	36.4	991.9	46.4	931.8	31.6	89.7	58.0	100.2	268.9	89.4	104.9
LILE	21462	35478	21688	15959	5401	20425	17827	14836	19462	25583	16230	17141	22317	21187	23387	12262	10429	24367	12205	12381	13630	16008
HFSE	833	3460	3607	3670	1579	5327	5202	781	5248	6260	430	558	5470	1032	7751	1138	1584	405	2232	1992	2729	4096
Eu*	0.07	0.76	0.82	0.81	0.82	0.82	0.86	0.45	0.83	0.81	0.50	0.36	0.82	0.43	0.89	0.58	0.43	0.64	1.25	1.21	1.04	0.88
Ce*	1.06	1.05	1.07	1.06	1.04	1.06	1.04	1.10	1.03	1.02	1.07	1.04	1.04	1.06	1.08	1.06	1.07	0.99	1.04	1.05	1.03	1.07
LR/HR	7.0	21.6	25.1	24.9	22.4	21.9	22.3	100.4	24.1	22.7	253.0	145.6	22.7	47.6	22.4	123.0	68.0	106.5	3.6	4.0	6.1	10.7

4.04, respectively, less than those of the Hul/Cpt-, chabazite-rich samples, and resembling the erionite-rich samples (Table 3). The monovalent cation contents $(Na_2O + K_2O)$ of the Hul/Cpt-rich samples were strongly and negatively correlated (r = 0.86) with the divalent cation contents (CaO + MgO). The divalent cation contents were generally greater than the monovalent cation contents (Table 3). Alkaline and alkaline earth element abundances as high as those of the Hul/Cpt-containing minerals were less common in the andesitic and basaltic lavas/tuffs than in the dacites of the Karacadağ volcanics. These elements were potentially mobile during the alteration of the tuffs and played an important role in the formation of new minerals, such as smectite, carbonate, and other zeolite minerals. Some trace elements, such as Ba, Sr, Rb, Ta, Th, U, and Y, were enriched in the zeolitic tuffs, mainly in the Hul/Cpt-rich tuffs compared with dacite (Table 4). The Sr and Ba contents were extremely high in some of the Hul/Cpt-rich samples and were strongly correlated (r = 0.89).

The zeolites in dacitic lavas have SiO_2/Al_2O_3 (4.32) and $(Na_2O+K_2O)/(MgO+CaO)$ (0.80) ratios that are similar to Hul/Cpt-rich (5.01, 0.71), erionite-rich (3.38, 0.91), chabazite-rich (4.05, 0.83), and vitric tuffs (4.32, 0.73) (Tables 3, 4), and different from basalt (3.17, 0.35), trachyandesite (3.54, 1.02), and hornblende andesite (3.73, 0.62), which crop out in the study area (Table 3). The SiO_2/Al_2O_3 and $(Na_2O + K_2O)/(CaO + MgO)$ mole ratios of the volcanic rocks, vitric tuffs, zeolitic tuffs, clays, and some zeolite-rich tuffs were plotted on a diagram which discriminates zeolite-rich tuffs, vitric tuffs, and dacites from the other volcanic rocks (Figure 8).

The REE contents of the zeolite-rich tuffs, tuffs, and bentonites are somewhat similar to those of dacites, basalts, and andesites. The REE of the samples were normalized to chondrites (Boynton, 1984). All of the normalized sample groups showed moderately similar REE patterns (Figure 9), and all of the sample groups were enriched in REE compared with the chondrites. The LREE of the Hul/Cpt-, erionite-, and chabazite-rich tuff showed similar trends while their HREE are different. The HREE were more enriched in the Hul/Cpt-rich samples and less enriched in the erionite- and chabazite-rich samples than in the other sample groups. The Eu anomaly was calculated using the formula $Eu/Eu^* = Eu_N/(Sm_N \times Gd_N)^{1/2}$ (Gromet et al., 1984). Strongly negative Eu/Eu* anomalies (Eu/Eu* <1) were observed in some of the samples (Table 4a−c). The Ce anomaly, represented as Ce/Ce*, was calculated with the formula $Ce/Ce^* = Ce_N/(La_N \times Pr_N)^{1/2}$ (Shimizu and Masuda, 1977). Ce anomalies were not observed in the zeolite- and smectite-rich samples (Table 4a-c, Figure 9). The chondrite-normalized LREE are enriched relative to HREE as clearly observed in erionite- and chabazite-rich tuffs, and showed virtually concave patterns in both the erionite- and chabazite-rich tuffs; HREE patterns of
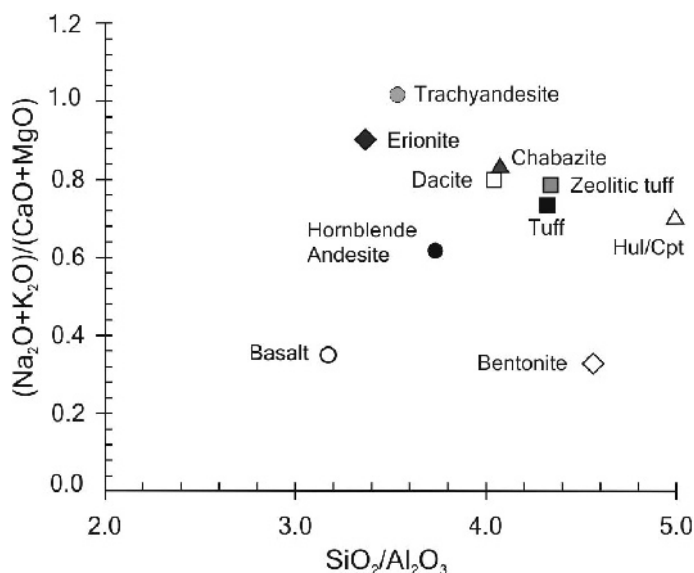
Figure 8. Variation of the ratio SiO_2/Al_2O_3 *vs.* $(K_2O+Na_2O)/(MgO+CaO)$ of the investigated samples and volcanic rocks in the study area.

the other sample groups are almost flat (Figure 9). The La/Y ratios of the Hul/Cpt-, erionite, and chabazite-rich tuffs are 10.71, 48.23, and 80.75, respectively. The amounts of HFSE, such as Hf, Nb, Ta, Ti, Zr, and Cr (Saunders *et al.*, 1980), and of some of the trace elements, such as Ba, Sr, Sc, Co, Ni, Cr, Th, and U in the Hul/Cpt-rich tuffs were similar to the vitric and zeolite-free tuffs and lavas (Table 4). The amounts of some of the trace elements (Ba, Sr) varied widely within the same section and from one section to another.

The SiO_2, Al_2O_3, and Fe_2O_3 contents of the dacite, which was used to represent parent rock, were within the expected limits for this type of rock (Middlemost, 1985) (Figure 10a). The chemical analyses of major-element oxides generally indicate that Fe, Ca, Na, Ti, Mn, and Cr

have been removed; and Mg, K, Al, and Si remain practically unchanged in the zeolite-rich and vitric tuffs. The bentonite is enriched in Mg, Ti, Cr, K, and in some samples Mn and Fe. Trace elements show different behaviors in different sample groups. The Ta and Th concentrations and in some samples the Sr, Cs, and Rb concentrations were elevated in most of the sample groups, whereas the Co, Ga, V, Y, and Zr concentrations were the most depleted (Figure 10b). The Hul/Cpt-rich samples were slightly enriched in Hf, Ta, Sr, Y, and Nb relative to the other zeolite-rich samples, possibly because of the partial release of mostly immobile elements from the rock. The elemental enrichment or depletion may result from the partial removal of some major and trace elements from the dacite precursor rock
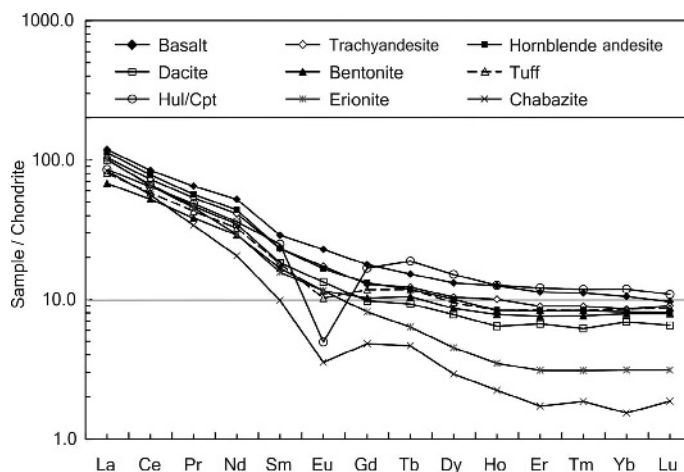
Figure 9. Chondrite-normalized *REE* patterns of the investigated sample groups and dacite (normalization values from Boynton, 1984). The data are from Table 4.

and the subsequent formation and precipitation of some zeolite and other minerals such as smectite and carbonates. The dacite-normalized *REE* patterns of the samples were almost parallel to each other and were characterized by virtually flat patterns, especially in the Hul/Cpt, tuff, and bentonite. The Eu anomalies were notable in all sample groups, except for the erionite-rich tuffs (Figure 10c). The Hul/Cpt-rich samples were
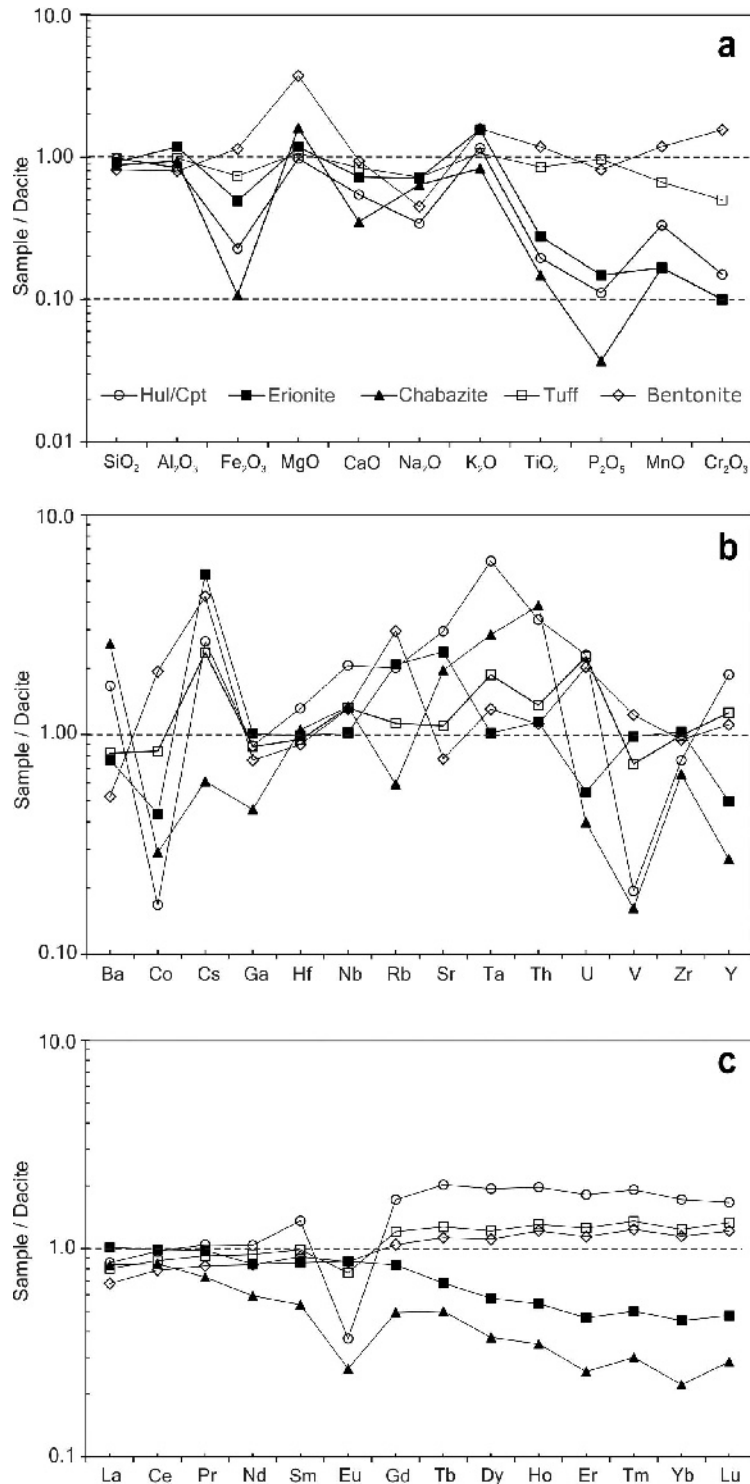
Figure 10. Dacite-normalized major-element oxides (a), trace (b) and *REE* (c) of the sample groups investigated.

Table 5. Oxygen and hydrogen isotopic compositions and paleotemperatures (°C) of Hul/Cpt, chabazite, analcime, and smectite.

Mineral	δD (‰)	$\delta^{18}O$ (‰)	Paleotemperature (°C)
Analcime	−70.0	16.0	72
Analcime	−72.7	15.9	72
Analcime	−75.0	19.8	51
Analcime	−93.3	15.9	72
Hul/Cpt	−74.9	14.0	71
Hul/Cpt	−85.7	15.1	64
Chabazite	−88.5	16.7	−
Hul/Cpt	−81.9	16.9	54
Hul/Cpt	−80.9	20.7	36
Hul/Cpt	−73.0	16.1	59
Smectite	−93.4	17.6	54
Smectite	−96.6	17.4	54
Smectite	−84.2	19.3	45
Smectite	−85.7	18.6	48

significantly enriched in the *HREE* and some of the *MREE*; this was less true of the zeolitic tuffs and bentonite; the chabazite- and erionite-rich tuffs were depleted of *HREE* and *MREE*.

Oxygen and deuterium isotope analyses were performed on the Hul/Cpt, chabazite, analcime, and smectite minerals that were found in abundance in the interlayered beds with the zeolite-rich tuffs. The O- and H-isotope compositions of the Hul/Cpt showed narrow ranges of +14.0 to +20.7‰ and from −73 to −85.7‰, respectively. The chabazite sample yielded similar O- and H-isotope compositions (*i.e.* +16.7‰ and −88.5‰, respectively). Analcimes have similar isotope compositions to the other zeolite minerals. Smectite samples had $\delta^{18}O$ and δD values of +17.4 to +19.3‰ and from −84.2 to −96.6‰, respectively (Table 5, Figure 11).

DISCUSSION

Changes in the zeolitic tuffs, bentonites, and carbonate rocks (limestone and dolomite) in the study area indicate that the pyroclastic rocks were altered in an alkaline, saline lacustrine basin that was rich in Ca and Mg ions. The Ca and Mg ions were partly sourced from the carbonate and ophiolitic rocks that surrounded the basin. The pyroclastic material consisted mainly of quartz and plagioclase (oligoclase and andesine) with some mica, and was altered to form zeolites and smectite. The following mineral associations were observed for the sequences: (a) Hul/Cpt + erionite ± opal-C/quartz; (b) Hul/Cpt + erionite + chabazite ± opal-C/quartz; and (c) smectite + calcite/dolomite with little or no Hul/Cpt and erionite (Table 1). The Hul/Cpt is the most abundant zeolite mineral and is associated
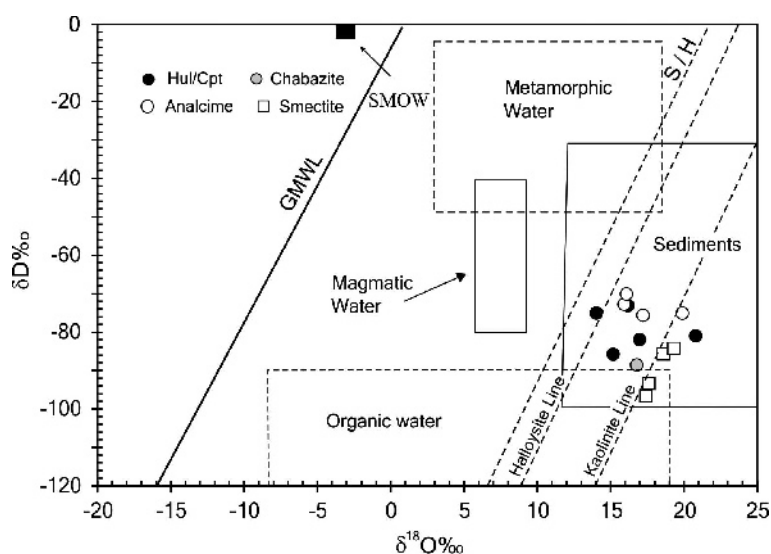
Figure 11. Summary of δD *vs.* $\delta^{18}O$ data for zeolite minerals and smectites on the diagram from Ece *et al.* (2013, and references therein).

with erionite, chabazite, and some analcime. The aforementioned associations showed mineralogical and chemical inhomogeneity, which reflected fluctuations in the lacustrine basin, where volcanic and sedimentary rocks with different compositions were deposited. The variable abundances of some trace elements such as Ba, Sr, Nb, Ta, Th Ga, Hf, and some of the Rb, U, Cs in the different layers, may, furthermore, be related to the enrichment of these elements in certain tuff layers (Table 4). These fluctuations may also have resulted from parent-rock composition, and elemental mobility due to climatic changes, alkalinity/pH, or the circulating/percolating meteoric water from the fractures/faults, and consequently dissolved constituents during the sedimentation process in the basin. The plagioclase compositions (oligoclase and/or andesine; Karakaya *et al.*, 2013) indicate that the Karacadağ volcanites, although consisting of a wide variety of volcanic rocks, were mainly dacitic and/or andesitic volcanics. The average SiO_2 and Al_2O_3 contents of the Hul/Cpt-rich tuffs and the vitric tuffs were 63.88 and 12.50 wt.% and 69.70 and 14.70 wt.%, respectively (Table 4). The SiO_2 contents of the dacite were similar to those of the Hul/Cpt-rich tuff and to the weakly altered tuff, whereas the Al_2O_3 content was slightly greater. The SiO_2/Al_2O_3 ratio of the dacitic rocks is 4.05, which is slightly less than that of the Hul/Cpt-rich tuff (5.01), the bentonite (4.41), and the vitric tuffs (4.32), but greater than erionite-rich tuff (3.38) and the same as the chabazite-rich tuff (4.05) (Table 4). Silica has been partially enriched and thus Si-rich phases such as opal-CT were formed during alteration. The CaO/Al_2O_3, Na_2O/Al_2O_3 and K_2O/Al_2O_3 ratios of the Hul/Cpt-rich tuffs were also similar to those of the vitric tuffs. The zeolite-free tuffs (vitric) contained slightly more SiO_2, Al_2O_3, Fe_2O_3, CaO, and TiO_2 and less Na_2O, K_2O, and MgO relative to the Hul/Cpt-rich tuffs due to their exposure to weak alteration, indicating that the alkaline and alkaline earth elements were mobile during the alteration of the tuffs in the basin (Table 4).

The *REE* patterns of the sample groups are characterized by *REE* enrichment relative to chondritic abundances (Figure 9). In particular, the *LREE* and some of the *MREE* were more enriched than the *HREE*. The *REE* trends of the precursors are similar to those of the basaltic lavas, andesitic lavas, bentonites, and of the vitric and zeolite-rich tuffs, indicating that the zeolite-rich tuffs probably originated from the dacitic lavas in the basin (Figure 9). These zeolite-rich tuffs demonstrated clearly negative Eu* anomalies at Hul/Cpt and chabazite, however, which were related to the removal of Ca following the partial destruction of the plagioclase which hosts most of the Eu (Figure 9). The strongly negative Eu anomaly of the zeolite and bentonite samples may have been inherited from the parent rocks during the alteration. Some of the leached Ca^{2+} was located on the exchange sites of the zeolite minerals and

smectite, and a large amount of the Ca^{2+} may have precipitated as calcite/dolomite in the basin. The enrichment of the *LREE* and the generally flat *HREE* patterns associated with the negative Eu anomaly are typical for felsic source rocks (Cullers and Graf, 1984). The remarkable similarity of the *REE* trends of all of the sample groups indicates that the zeolite minerals were derived from a common parent rock of the Karacadağ volcanic suite, mainly through diagenetic alteration processes of the dacitic volcaniclastics. The depletion of some of the *MREE* and of most of the *HREE* in the erionite- and chabazite-rich tuffs relative to the Hul/Cpt-rich tuffs may be related to the different absorption capacities and/or channel dimensions of the zeolite minerals. Dacitic rocks, the likely parent rocks, were characterized by *REE* patterns with relatively steep negative slopes (La/Yb = 20.17) and with no Eu anomaly (Eu/Eu*$_{CN}$ = 1.00) (Figure 9, Table 3). The *HREE* and some of the *MREE* were significantly depleted in the erionite- and chabazite-rich tuffs, while the Hul/Cpt-rich tuffs were clearly enriched in the same elements. The Hul/Cpt-rich tuffs and smectitic bentonite were enriched in different *REE*s, especially *HREE* with dacite-normalized behavior unlike those of the other zeolite-rich samples (Figure 10c). The enrichment or leaching of some of the *MREE* and in particular of *HREE* relative to dacite suggests that these elements might have been mobilized as complexes during alteration and may be concentrated in the Hul/Cpt and smectite structure. Alternatively, the greater degree of *REE* fractionation may result from the greater solubility of the *HREE*, compared with *LREE*, due to preferential complexation with carbonate ligands in alkaline solutions (Lazaro *et al.*, 1994 and references therein).

Zeolitization can occur both in open and closed hydrologic systems (Langella *et al.*, 2001). The zeolitic tuffs and smectite were formed from diagenetic alterations, mainly of dacitic tuff/glass, and from the interactions of water in a suitable hydrological environment (Yanev *et al.*, 2006). If the system is suitably closed, alkalis and alkaline earth elements are leached during hydration, which increases the pH and salinity (Hay and Sheppard 1977). During the early stages, when alkalinity and salinity are low, this process promotes the formation of smectite with high $(Na^+ + K^+)/H^+$ ratios, resulting in the occurrence of zeolites (Christidis *et al.*, 1995 and references therein).

The chemistry of the water is controlled mainly by evaporation, and the water evolution is controlled largely by processes that cause highly concentrated alkaline brine in a closed hydrological system (Eugster, 1970). The alkalinity is related to significant Ca^{2+} and HCO_3^- activity in solution; thus, the carbonate activity can lead to precipitation of calcite (Langella *et al.*, 2001). Calcite precipitates when the lake water is diluted while the dolomite precipitates if the lake water is more alkaline, and when the interaction of the glass with

aqueous fluid controls the chemistry and pH of the basin. The presence of some zeolite minerals in the voids/cavities of the pumice/glass may indicate that the minerals formed from dissolved ions of the volcanic glass during the hydration process. The hydration of the tuffs may have resulted in the formation of zeolite, K-feldspar, smectite, and opal-CT in a relatively open lacustrine environment with different alkalinities. The saturation of the alkalis and alkaline earth elements in the basin may have led to the formation of zeolite minerals rather than smectite after glass dissolution during which the pH increased. The increase in the Mg and, to a lesser extent, Fe contents relative to the precursor rock in the bentonitic smectite during alteration promotes the formation of smectite (Christidis, 1998).

The formation of silica-rich zeolite (*e.g.* clinoptilolite, mordenite, some erionite) may have occurred when the pH of the fluids was between 7 and 9 (Sheppard *et al.*, 1988). The presence of amorphous silica with smectite and gypsum, hexahydrite, and carbonate minerals indicates an increased dissolved-silica activity and a high pH. The textural relationships, which were identified by polarized-light microscopy and SEM investigations, suggest that the zeolites are alteration products that formed mainly from the partial or complete dissolution of feldspar minerals and glassy components (shards and vitric ash) in the dacitic tuffs. The smectite was formed as a late phase in small cavities or as overgrowths on zeolites. The exchangeable-cation contents of the smectites varied over a wide range; some were rich in Na or Ca. The subsequent hydrolysis of tuff/glass and the formation of smectite may have occurred at high pH, under high-SiO_2 activities, and (Na + K)/H$^+$ activity ratios (Hay, 1966; Hay and Sheppard, 1977, 2001; Hay and Guldman, 1987; Tsolis-Katagas and Katagas, 1990).

Smectite is present in trace amounts in most of the zeolite-rich samples; in strata in which smectite is predominant, however, low alkali activity probably prevailed in the study area. The Hul/Cpt minerals and smectite are related directly to each other, and the occurrence of smectite superposed upon the Hul/Cpt crystals suggests that some of the smectite formed from liquid remaining after the formation of Hul/Cpt. The SEM observations further indicated that smectite is not only formed from volcanic material as an authigenic mineral, but also from Hul/Cpt minerals as metastable products due to changes in the basin chemistry (Figure 7f). The formation of smectite from volcanic materials has been shown in many examinations of natural materials and in experimental studies (*e.g.* Caballero *et al.*, 1991; Tomita *et al.*, 1993; Langella *et al.*, 2001; Karakaya *et al.*, 2011). Tomita *et al.* (1993) investigated clay minerals and zeolites from volcanic materials below temperatures of ~100ºC and observed that smectite formed at a relatively low glass-to-NaOH

ratio. The formation of smectite from an acidic to intermediate precursor rock required the removal of excess Si and alkalis at low temperature and under basic conditions. A semi-open system would support mineral formation with Hul/Cpt-rich tuffs and bentonite interlayers. If the system was fully open, all Si and alkalis would be removed and smectite would be the only phase present (Kitsopoulos, 1997). Smectite and amorphous silica were also identified in vitric tuff samples. Although some of the bentonite, which contains almost the same amount of alkalis as do the tuffs, and marl layers interlayered with the vitric tuffs, contained no zeolite minerals, the formation of zeolite from the volcanic material may have been interrupted occasionally due to changing of environmental conditions or because the glass was mostly transformed into smectite and some carbonate minerals. The abundance of Ca-rich Hul/Cpt and other zeolite minerals that generally occur in the porous tuffs and the scarcity of the other zeolite minerals in some of the smectitic bentonite layers indicate that the minerals were mainly formed from altered parent volcanic materials in a low-salinity environment. Zeolite minerals formed mainly from saturated solutions which were circulated through the pores. Thin silica (opal-CT) layers (1−5 cm thick) or lenses may have been formed by transformation of the glass into smectite. The association of calcite, dolomite, and Hul/Cpt-rich samples in some samples and their large Ca and Mg contents compared with the likely precursor rocks (Table 3, 4) suggest that the fluids rich in Ca and Mg were mainly derived from the surrounding carbonate and ophiolitic rocks.

Open hydrological basins are the most appropriate environment for the zeolitization of volcanic materials (Hay and Sheppard, 1977; Sheppard and Hay, 2001). The aereal distributions, lithological properties, and mineralogical and chemical variations among the sediments studied reveal that the depositional environments were probably slightly open hydrological systems at some point rather than completely open systems. (1) The deposits of the Aktepe formation were similar to saline-alkaline lake deposits because of the presence of zeolitic tuffs, limestones, and some evaporite minerals in the succession. A playa environment developed in Tuzgölü lake, a closed saline alkaline lake that is mostly isolated from external basins and is the largest salt lake in Turkey. (2) The presence of a few saline minerals including gypsum, halite, and hexahydrite indicated high levels of evaporation. Calcite and dolomite were abundant in the carbonate beds that are interlayered with the smectitic bentonite layers and Hul/Cpt-rich tuffs. Wali *et al.* (2009) conducted experimental studies and found that hexahydrite is stable between 50 and 65ºC. This mineral precipitates in progressively evaporated playa lakes from hypersaline brines (Eugster and Hardie, 1978; Eugster, 1980). (3) Due to faulting and folding caused by active tectonics, lateral zonation was

not observed, although weak vertical zonation was observed at the outcrop scale. Smectite- and carbonate-rich beds (Hul/Cpt + erionite + chabazite) were found at the top, and a Hul/Cpt horizon (+ smectite) containing analcime was observed at the bottom of the sequence. Almost pure limestone overlies the sequence. Between these lithologies, unaltered, highly compacted vitric tuff (0.5−2 mm grain size) and some lava layers (10−50 cm) occur, which may indicate that they were above the water levels due to occasionally lower water levels in the closed basin. (4) The zeolite minerals, including analcime, Hul/Cpt, chabazite, erionite, and rarely phillipsite, usually form in a relatively closed hydrological system (Surdam, 1977; Hay, 1978; Surdam and Sheppard, 1978; Hay and Guldman, 1987; Langella *et al.*, 2001, and references therein), such as the area discussed in the present study. Surdam and Sheppard (1978) suggested that the zeolite minerals are common in saline, alkaline-lake deposits such as in the present study area. The smectite that lined the relict glass and partially altered glass with Hul/Cpt ± erionite indicated a relatively closed hydrological system in which the excess silica was not released into the basin. The alkalinity of the basin may have been controlled mainly by the precipitation of calcite and dolomite and by dissolution of glass. Broxton *et al.* (1987) indicated that the occurrence of silica-rich zeolites (clinoptilolite and some heulandite) is favored by pH values that are close to or slightly higher than neutral (7−9). Chabazite is probably formed when the basin is less alkaline and saline in the outer parts of the lake where freshwater flows (Langella *et al.*, 2001). The evaporitic minerals, analcime, and authigenic K-feldspar, indicate low–medium and some high salinities and that the pH was <9 during zeolitization (Surdam and Parker, 1972), consistent with salt water circulating in the pores.

The δ¹⁸O and δD values plotted are far from the meteoric water line and meteoric water in the Konya region, and depleted δD and enriched δ¹⁸O values were determined (Figure 11). The values are also located away from igneous- and metamorphic-water areas. Smectites lie close to the smectite/halloysite line and away from the meteoric water line that may be formed at low temperature (Sheppard *et al.*, 1969). The isotope data from the minerals may reflect differences in temperature of mineral formation within the basin, and isotopic compositions may be modified by evaporation (Table 5; Figure 11). The δ¹⁸O values of analcimes are between 15.9 and 19.8‰, similar to values of sedimentary analcimes (16.6−24.5‰) rather than those of hydrothermal analcimes (8.7−14.3‰) formed at low temperatures (0−50ºC) (Karlson and Clayton, 1990). The δ¹⁸O content of the meteoric water in the Konya region is −8.5‰ (Bayarı *et al.*, 2009). The isotopic temperatures of the Hul/Cpt, analcime, and smectite were calculated using the formula described by Nähr *et al.* (1998), Karlson and Clayton (1990), and Escande

(1984), respectively (Table 5). The δ¹⁸O value of chabazite is slightly lower than those of the Hul/Cpt minerals indicating that chabazite precipitated from partially oxygen-depleted water and that its formation temperature is similar to that of the Hul/Cpt. The calculated isotopic temperatures of the analcimes and Hul/Cpt range from 51 to 72ºC and from 36 to 71ºC, respectively. The temperatures indicate that the zeolite minerals formed at moderately low temperatures, mostly due to diagenetic influences, similar to the temperatures of formation in the Yamato Basin (33−62ºC) (Nähr *et al.*, 1998), and slightly lower than the temperatures determined by Gottardi (1989) (41−91ºC). The temperatures of formation of smectites are between 48 and 54ºC. Savin *et al.* (1993) determined oxygen isotope data from smectite and indicated that the temperature of formation of diagenetic smectite is <45ºC, close to the results determined here. The temperature determined in the present study is also consistent with the precipitation temperature of hexa-hydrite that was observed on the surface of Hul/Cpt-rich tuff layers and is similar to the values of ~80ºC given by Karlsson and Clayton (1990) for clinoptilolite. The O- and H-isotope compositions of Hul/Cpt resemble the diagenetic clinoptilolite values presented by Karlsson (2001) who indicated that the low values were related to the occurrence of more variations in ¹⁸O-depleted fluids in the terrestrial hydrothermal (meteoric water) environment. Almost all of the isotope values determined were between the supergene/hypogene and the smectite lines presented by Sheppard *et al.* (1969) which indicated that the isotopic compositions of the minerals were in equilibrium with meteoric waters at 20ºC.

The greater δD values in all of the analcimes and in most of Hul/Cpt than those of chabazite and smectite suggest that the former minerals were precipitated from more evaporated water. The isotopic compositions of the smectite and zeolite minerals are similar, and may be influenced by many factors, *e.g.* isotopic composition of the precursor rocks, meteoric water, and temperature in the basin when the mineral precipitated. The area studied is a relatively closed, hydrologically speaking, lake basin which loses the majority of its water through evaporation and thus is more enriched in heavy isotopes than are 'open' lakes (Huang and Pang, 2012; Steinman and Abbott, 2013). The meteoric water was in contact with the precursor rocks which contain more oxygen than hydrogen, and later, during precipitation and evaporation, substantial isotopic exchange may have occurred in the neoformed minerals. The isotopic data of the zeolite minerals plot close to the smectites, suggesting that the zeolites form under similar conditions. The transformation of the minerals from glass, and the similar micromorphological properties of the Hul and Cpt indicate that they formed under similar conditions and from similar precursor rocks and/or in fluids with similar compositions. The results also indicated that high

temperatures are not a significant factor in the formation of authigenic zeolites and smectite because the minerals were formed at low to moderately low temperatures.

CONCLUSIONS

Hul/Cpt is the main zeolite mineral in the study area and was found to coexist with erionite, occasionally with chabazite, and rarely with analcime. The parallel chondrite-normalized *REE* patterns of the Hul/Cpt-, chabazite- and erionite-rich tuffs indicated that most of the zeolite minerals were mostly formed from the alteration of felsic to intermediate rocks in Karacadağ volcanics in a closed hydrologic basin. The variability of some major, HFSE, LILE, and *REE* from the precursor rocks of the sample suites probably indicates variation of the evaporative conditions and alteration of volcanic material. The clearly different La/Yb ratios of the minerals indicate that the *LREE* are more enriched in the Hul/Cpt-rich tuffs than the other elements. The dacite-normalized *REE* and some of the trace-element patterns in the zeolite-rich minerals and vitric tuffs are analogous to each other but are depleted in the chabazite- and erionite-rich samples. The zeolitic tuffs are in contact with vitric tuffs in which the devitrification of the ash resulted in the formation of minor K-feldspar during later diagenesis.

The zeolitic tuff layers investigated contained ~40−90% Hul/Cpt and chabazite, and the thickness and lateral continuity of the layers may have economic implications for certain applications. The Hul/Cpt and chabazite minerals were formed at between 34.2ºC and 67.0ºC, and the smectites were formed at between 45 and 54ºC. The isotopic compositions of the minerals suggest that the minerals formed at low to moderately low temperatures under similar saline alkaline-basin conditions and/or in fluids with similar composition in a partially open or closed basin.

REFERENCES

Bayarı, C.S., Özyurt, N.N., and Kilani, S. (2009) Radiocarbon age distribution of groundwater in the Konya Closed Basin, central Anatolia, Turkey. *Hydrogeology Journal*, **17**, 347−365.

Boynton, W.V. (1984) Geochemistry of rare earth elements: meteorite studies. Pp. 63−114 in: *Rare Earth Element Geochemistry* (P. Henderson, editor). Elsevier, Amsterdam.

Broxton, D.E., Bish, D.L., and Warren, R.E. (1987) Distribution and chemistry of diagenetic minerals at Yucca Mountain, Nye County, Nevada. *Clays and Clay Minerals*, **35**, 89−110.

Caballero, E., Reyes, E., Huertas, F., Linares, J., and Puzzuoli, A. (1991) Early-stage smectites from pyroclastic rocks of Almena (Spain). *Chemical Geology*, **89**, 353−358.

Christidis, G. (1998) Comparative study of the mobility of major and trace elements during alteration of an andesitic and a rhyolitic rock to bentonite in the islands of Milos and Kimolos, Aegean, Greece. *Clays and Clay Minerals*, **46**, 379−399.

Christidis, G., Scott, R.W., and Marcopoulos, T. (1995) Origin of the bentonite deposits of Eastern Milos, Aegean, Greece. Geological, mineralogical, and geochemical evidence. *Clays and Clay Minerals*, **43**, 63−77.

Cullers, R.L., and Graf, J.L. (1984) Rare earth elements in igneous rocks of the continental crust: Predominantly basic and ultrabasic rocks. Pp. 275−308 in: *Rare Earth Element Geochemistry* (P. Henderson, editor). Elsevier, Amsterdam.

Escande, M.A., Decarreau, A., and Labeyrie, L. (1984) Etude expérimentale de l'échangeabilité des isotopes de l'oxygène des smectites. *Comptes Rendus de l'Académie des Sciences*, **229**, 707−710.

Esenli, F. and Kumbasar, I. (1998) X-ray diffraction intensity ratios $I(111)/I(\bar{3}11)$ of natural heulandites and clinoptilolites. *Clays and Clay Minerals*, **46**, 679−686.

Esenli, F. and Özpeker, I. (1993) Zeolitic diagenesis of Neogene basin and the mineralogy of heulandite-clinoptilolite around Gördes. *Geological Bulletin of Turkey*, **8**, 1−18.

Esenli, F. and Sirkecioğlu, A. (2005) The relationship between zeolite (heulandite-clinoptilolite) content and the ammonium-exchange capacity of pyroclastic rocks in Gördes, Turkey. *Clay Minerals*, **40**, 557−564.

Eugster, H.P. (1970) Chemistry and origin of the brines from Lake Magadi, Kenya. *Mineralogical Society of America Special Paper*, **3**, 215−235.

Eugster, H.P. (1980) Geochemistry of evaporitic lacustrine deposits. *Annual Review of Earth and Planetary Sciences*, **8**, 35−63.

Eugster, H.P. and Hardie, L.A. (1978) Saline lakes. Pp. 237−289 in: *Lakes: Chemistry, Geology, Physics* (A. Lerman, editor). Springer, New York.

Feng, X. and Savin, S.M. (1993) Oxygen isotope studies of zeolites − stilbite, analcime, heulandite, and clinoptilolite, III: Oxygen isotope fractionation between stilbite and water or water vapor. *Geochimica et Cosmochimica Acta*, **57**, 4239−4247.

Gottardi, G. (1989) The genesis of zeolites. *European Journal of Mineralogy*, **1**, 479−487.

Görür, M.N., Oktay, F.Y., Seymen, O., and Şengör, A.M.C. (1984) Paleotectonic evolution of the Tuzgölü basin complex, Central Turkey: sedimentary record of a Neo-Tethyan closure. Pp. 467−482 in: *The Geological Evolution of the Mediterranean* (J.E. Dixon and A.H.F. Robertson, editors). Geological Society, London.

Gromet, L.P., Dymek, R.F., Haskin, L.A., and Korotev, R.L. (1984) The North American shale composite: Its composition, major and trace element characteristics. *Geochimica et Cosmochimica Acta*, **48**, 2469−2482.

Gündoğdu, M.N. (1982) Neojen yaşlı Bigadiç sedimanter baseninin jeolojik, mineralojik ve jeokimyasal incelenmesi. PhD thesis, Hacettepe University, Ankara, Turkey, 386 pp.

Gündoğdu, M.N., Yalçın, H., Temel, A., and Clauer, N. (1996) Geological, mineralogical and geochemical characteristics of zeolite deposits associated with borates in the Bigadiç Emet and Kırka Neogene lacustrine basins, western Turkey. *Mineralium Deposita*, **31**, 492−513.

Gürer, O.F. and Aldanmaz, E. (2002) Origin of the Upper Cretaceous-Tertiary sedimentary basins within the Tauride-

Anatolide platform in Turkey. *Geological Magazine*, **139**, 191–197.

Hay, R.L. (1966) Zeolites and zeolitic reactions in sedimentary rocks. *Geological Society of America Special Paper*, **85**, 130 pp.

Hay, R.L. (1978) Geologic occurrence of zeolites. Pp. 135–143 in: *Natural Zeolites: Occurrence, Properties, Use* (L.B. Sand and F.A. Mumpton, editors). Pergamon, Elmsford, New York.

Hay, R.L. and Guldman, S.G. (1987) Diagenetic alteration of silicic ash in Searles Lake, California. *Clays and Clay Minerals*, **35**, 449–457.

Hay, R.L. and Sheppard, R.A. (1977) Zeolites in open hydrologic systems. Pp. 93–102 in: *Mineralogy and Geology of Natural Zeolites* (F.A. Mumpton, editor). Short Course Notes **4**, Mineralogical Society of America, Washington, D.C.

Hay, R.L. and Sheppard, R.A. (2001) Occurrence of zeolites in sedimentary rocks: an overview. Pp. 217–234 in: *Natural Zeolites: Occurrence, Properties, Applications* (D. Bish and D. Ming, editors). Reviews in Mineralogy, **45**, Mineralogical Society of America, Washington.

Helvacı, C., Stamatakis, M.G., Zagouroğlou, C., and Kanaris, J. (1993) Borate minerals and related authigenic silicates in northeastern Mediterranean late Miocene continental basins. *Exploration and Mining Geology*, **2**, 171–178.

Hernandez, J.E.G., Notario del Pino, J.S., Gonzalez Martin, M.M., Hernan Reguera, F., and Rodriguez Losada, J.A. (1993) Zeolites in pyroclastic deposits in southeastern Tenerife (Canary Islands). *Clays and Clay Minerals*, **41**, 521–526.

Huang, T.M. and Pang, Z.H. (2012) The role of deuterium excess in determining the water salinisation mechanism: A case study of the arid Tarim River Basin, NW China. *Applied Geochemistry*, **27**, 2382–2388.

Iijima, A. (1978) Geological occurrences of zeolites in marine environments. Pp. 175–198 in: *Natural Zeolites: Occurrence, Properties, Use* (L.B. Sand and F.A. Mumpton, editors). Pergamon Press, New York.

Innocenti, F., Mazzuoli, R., Pasquare, G., Radicati Di Brozolo, F., and Villari, L. (1975) The Neogene calcalkaline volcanism of central Anatolia: Geochronological data on Kayseri-Niğde area. *Geological Magazine*, **112**, 349–360.

Kaçmaz, H. and Köktürk, U. (2004) Geochemistry and mineralogy of zeolitic tuffs from the Alaçatı (Ceşme) area, Turkey. *Clays and Clay Minerals*, **52**, 705–713.

Karakaya, N. (2009) REE and HFS element behaviour in the alteration facies of the Erenler Dağı volcanics (Konya, Turkey) and kaolinite occurrence. *Journal of Geochemical Exploration*, **101**, 185–208.

Karakaya, M.Ç., Karakaya, N., and Küpeli, Ş. (2011) Mineralogical and geochemical properties of the Na- and Ca-bentonites of Ordu (N.E. Turkey). *Clays and Clay Minerals*, **59**, 75–94.

Karakaya, N., Karakaya, M.Ç., and Yavuz, F. (2012) Investigation of mineralogic, geochemical and some technologic properties of zeolite occurrences in around of Kulu (Konya) and Haymana (Ankara). TÜBİTAK 109Y301, 200 pp.

Karakaya, N., Karakaya, M.Ç., and Temel, A. (2013) Mineralogical and chemical properties and the origin of two types of analcime in SW Ankara, Turkey. *Clays and Clay Minerals*, **61**, 231–257.

Karlsson, H.R. (2001) Isotope geochemistry of zeolites. Pp. 163–205 in: *Natural Zeolites: Occurrence, Properties, Applications* (D.L. Bish and D.W. Ming, editors). Reviews in Mineralogy and Geochemistry, **45**, Mineralogical Society of America and Geochemical Society, Washington.

Karlsson, H.R. and Clayton, R.N. (1990) Oxygen and hydrogen isotope geochemistry of zeolites. *Geochimica et Cosmochimia Acta*, **54**, 1369–1386.

Kitsopoulos, K.P. (1997) The genesis of a mordenite deposit by hydrothermal alteration of pyroclastics on Polyegos island, Greece. *Clays and Clay Minerals*, **45**, 632–648.

Kurt, H., Asan, A., and Ruffet, G. (2008) The relationship between collision-related calcalkaline, and within-plate alkaline volcanism in the Karacadağ Area (Konya-Türkiye, Central Anatolia). *Chemie der Erde*, **68**, 155–176.

Langella, A., Cappeletti, P., and de'Gennaro, M. (2001) Zeolites in closed hydrologic systems. Pp. 235–260 in: *Natural Zeolites: Occurrence, Properties, Applications* (D.L. Bish and D.W. Ming, editors). Reviews in Mineralogy and Geochemistry, **45**, Mineralogical Society of America and Geochemical Society, Washington.

Lazaro, B.B., Abad, C.A., Fernandez-Nieto, C., and. Gonzalez Lopez, J.M. (1994) Mineralogy and geochemistry of Miocene deposits at Alcubierre Sierra, central sector of the Ebro Basin, Spain. *Clay Minerals*, **29**, 341–400.

Middlemost, E. A. K. (1985) Magmas and magmatic rocks. An Introduction to Igneous Petrology Longman, London.

Ming, D.W. and Dixon, J.B. (1987) Technique for the separation of clinoptilolite from soils. *Clays and Clay Minerals*, **35**, 469–472.

Mumpton, F.A. (1999) La roca magica: Uses of natural zeolites in agriculture and industry. *Proceedings of the National Academy of Sciences of the United States of America*, **96**, 3463–3470.

Nähr, T.H., Botz, R., Bohrmann, G., and Schmidt, M. (1998) Oxygen isotopic composition of low-temperature authigenic clinoptilolite. *Earth and Planetary Science Letters*, **160**, 369–381.

Okay, A.I., Tansel, İ., and Tüysüz, O. (2001) Obduction, subduction and collision as reflected in the Upper Cretaceous–Lower Eocene sedimentary record of western Turkey. *Geological Magazine*, **138**, 117–142.

Pasquar, G., Poli, S., Vezzoli, L., and Zanchi, A. (1988) Continental arc volcanism and tectonic setting in Central Anatolia, Turkey. *Tectonophysics*, **146**, 217–230.

Passaglia, E. and Sheppard, R.A. (2001) Crystal chemistry of zeolites. Pp. 69–116 in: *Natural Zeolites: Occurrence, Properties, Applications* (D.L. Bish and D.W. Ming, editors). Reviews in Mineralogy and Geochemistry **45**, Mineralogical Society of America and Geochemical Society, Washington, D.C.

Rollinson, H. (1993) *Using Geochemical Data: Evaluation, Presentation, Interpretation.* Longman Scientific and Technical, Harlow, Essex, UK.

Şahin, M.B. (2007) Orta Anadolu'da belirlenen önemli bir şabazit oluşumu ve mineralojik özellikleri. *MTA Dergisi*, **135**, 31–44.

Saunders, A.D., Tarney, J., Marsh, N.G., and Wood, D.A. (1980) Ophiolites as ocean crust: a geochemical approach. Pp. 193–204 in: *Ophiolites: Proceedings of the International Ophiolite Symposium* (A. Panayiotou, editor). Ministry of Agriculture and Natural Resources, Cyprus, 1979. Geological Survey Department, Cyprus.

Savin, S., Tsirambides, A., Kassoli-Fournaranki, A., and Filippidis, A. (1993) Oxygen-isotope evidence for the alteration of the Eocene zeolite-bearing volcaniclastic sediments of Metaxades, Thrace, Greece. Zeolite '93, Idaho, pp. 180–181.

Sharp, Z.D. (1990) Laser-based microanalytical method for the in situ determination of oxygen isotope ratios of silicates and oxides. *Geochimica et Cosmochimica Acta*, **54**, 1353–1357.

Sheppard, R.A. and Hay, R.L. (2001) Formation of zeolites in open hydrologic systems. Pp. 261–276 in: *Natural Zeolites: Occurrence, Properties, Application* (D.L. Bish and D.W.

Ming, editors). Reviews in Mineralogy and Geochemistry, **45**. Mineralogical Society of America and Geochemical Society, Washington, D.C.

Sheppard, S.M.F., Nielsen, R.L., and Taylor, H.P., Jr. (1969) Oxygen and hydrogen isotope ratios of clay minerals from porphyry copper deposits. *Economic Geology*, **64**, 755−777.

Shimizu, H. and Masuda, A. (1977) Cerium in chert as an indication of marine environment of its formation. *Nature*, **266**, 346−348.

Snellings, R., Haten van T., Machiels, L., Mertens, G., Vandenberghe, N., and Elsen, J. (2008) Mineralogy, geochemistry, and diagenesis of clinoptilolite tuffs (Miocene) in the central Simav graben, Western Turkey. *Clays and Clay Minerals*, **56**, 622−632.

Surdam, R.C. (1977) Zeolites in closed hydrologic systems. Pp. 65−91 in: *Mineralogy and Geology of Natural Zeolites* (F.A. Mumpton, editor). Reviews in Mineralogy, **4**. Mineralogical Society of America, Washington, D.C.

Surdam, R.C. and Parker, R.B. (1972) Authigenic alumino-silicate minerals in the tuffaceous rocks of the Green River Formation, Wyoming. *Geological Society of America Bulletin*, **83**, 689−700.

Surdam, R.C. and Sheppard, R.A. (1978) Zeolites in saline, alkaline-lake deposits. Pp. 145−174 in: *Natural Zeolites: Occurrence, Properties, Use* (L.B. Sand and F.A. Mumpton, editors). Pergamon Press, Elmsford, New York.

Steinman, B.A. and Abbott, M.B. (2013) Isotopic and hydrologic responses of small, closed lakes to climate variability: Hydroclimate reconstructions from lake sediment oxygen isotope records and mass balance models. *Geochimica et Cosmochimica Acta*, **105**, 342−359.

Temel, A. and Gündoğdu, M.N. (1996) Zeolite occurrences and the erionite-mesothelioma relationship in Cappadocia, central Anatolia. *Mineralium Deposita*, **31**, 539−547.

Temel, A., Gündoğdu, M.N., and Gourgaud, A. (1998) Petrological and geochemical characteristics of Cenozoic high-K calc-alkaline volcanism in Konya, Central Anatolia, Turkey. *Journal of Volcanology and Geothermal Research*, **85**, 327−354.

Tomita, K., Yamane, H., and Kawano, M. (1993) Synthesis of smectite from volcanic glass at low temperature. *Clays and Clay Minerals*, **41**, 655−661.

Tsolis-Katagas, P. and Katagas, C. (1990) Zeolitic diagenesis of Oligocene pyroclastic rocks of the Metaxades area, Thrace, Greece. *Mineralogical Magazine*, **54**, 95−103.

Tucker, M.E. (1988) *Techniques in Sedimentology*. Blackwells. Oxford. 394 pp.

Uğuz, F.M., Turhan, N., Bilgin, A.Z., Umut, M., Şen, A.M. ve Acarlar, M. (1999) Kulu (Konya)-Haymana (Ankara) ve Kırıkkale dolayının jeolojisi. MTA Rapor No: 10399, Ankara (unpublished report).

Wali, A.M., Dardir, A.A. and Elsheikh, R.M (2009) Mineralogy and mineral successions crystallization of the waste residual brines. 9th World Salt Symposium, Beijing.

Whitney, D.L. and Evans, B.W. (2010) Abbreviations for names of rock-forming minerals. *American Mineralogist*, **95**, 185−187.

Winchester, J.A. and Floyd, P.A. (1977) Geochemical discrimination of different magma series and their differentiations products using immobile elements. *Chemical Geology*, **20**, 325−340.

Yanev, Y., Boev, B., Innocenti, F., Manetti, P., Pecskay, Z., Tonarini, S., and, D'Orazio, M. (2006) Ultrapotassic to potassic Late Neogene volcanic rocks in Macedonia: Mineralogy, geochemistry, and age. *Proceedings of the XVIIIth Congress of the Carpathian-Balkan Geological Association, Belgrade*, pp. 666−669.